Master Thesis, Department of Geosciences

Diagnostics of eddy diffusivities in high resolution regional ocean models

John Erik C Skogtvedt

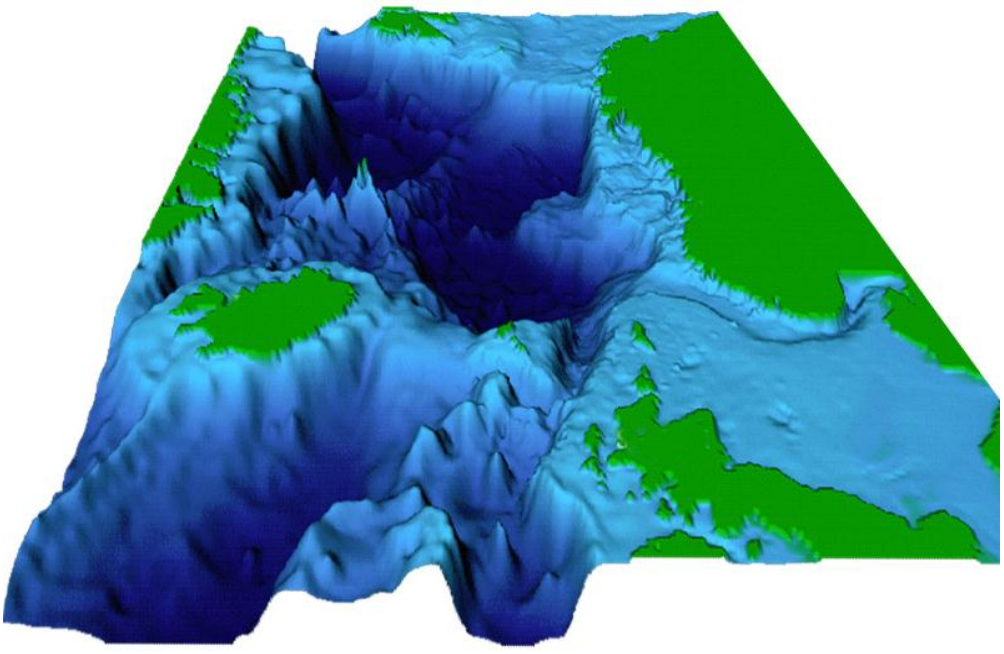

UNIVERSITY OF OSLO

FACULTY OF MATHEMATICS AND NATURAL SCIENCES

Diagnostics of eddy diffusivities in high resolution regional ocean models

An evaluation of diffusivity closures

John Erik C Skogtvedt

Master Thesis in Geosciences/Oceanography

Department of Geosciences

Faculty of Mathematics and Natural Sciences

University of Oslo

14th of June, 2011

The cover illustration is borrowed from Department of Mathematics, University of Oslo.

Acknowledgements

I would like to thank Professor Lars Petter Røed for introducing me to the field of physical oceanography. His encouragement, support, and great insight have both helped and inspired me through the studies.

Also thanks to Pål Erik Isachsen, for his excellent help with both technical and theoretical issues along the way. I have benefited immensely by conversations with him as the work progressed.

Abstract

A collection of closure schemes for eddy diffusivities κ, appropriate for isopycnal diffusion (Redi 1982) and stirring (Gent-McWilliams 1990), are tested and evaluated in comparison to output from a high resolution regional ocean model. This study is supplementary to that of Eden et al. (2008), where the effect of various choices for κ in general circulation climate models were compared with climatological data. In order to obtain a viable diffusivity diagnosis (with positive diffusivities) directly from the resolved eddy fluxes, rotational components should be removed. For this we attempt the method proposed by Medvedev & Greatbatch (2004), which happens to cause unexpected rise to negative diffusivities. However, in contrast to many previous studies, a strong flux-gradient relationship between eddy fluxes and mean fields were found, affording positive κ. Taking divergences confirms a solid correlation, indicating that rotational fluxes actually did not thwart the raw diagnostics to a significant level in this experiment. The diagnostic is therefore taken to be a proper frame of reference for comparing the various closures for distributions of eddy diffusivity. These closures are generally found to produce reasonable, but lacking, approximations to the diagnosed distribution of κ. A Ferrari-Nikarushin--suppression (2010) is shown to yield small but noticeable improvements. Some of the proposed tuning parameters seem to overestimate the overall intensity of diffusivities. The closure of Visbeck et al. (1997) performs well in respect to depth averaged distribution of κ, but its depth invariance motivates for choices of other closures; our diagnosis assert to a depth decaying diffusivity, so we also suggest a modification to this closure. None of the closures appears to dominate in quality in all aspects, and should be chosen in accordance with the physical application.

Table of Contents

Section 1: Introduction

The ocean is a system of vast dynamical complexity ranging over a large number of space-time scales, from the molecular scale to the large scale flow of the thermohaline circulation of the World Ocean. We face challenges of how to describe this system, both physically and then in turn how to express these physics on a discrete numerical grid. As we are privy to very limited information about the fluid and the huge diversity of processes therein, and due to the fact that our models to varying degree fail to resolve the smaller scale (turbulent) flow, a statistical approach of (Eulerian) averaged dynamics is necessary.

The resulting averaged equations naturally contain less information than the original equations. Oceanographic literature has traditionally regarded large scale flow dynamics separately from dynamics on smaller scales, based on the hypothesis that there are little interaction between the two regimes. This is at best a questionable assumption, and does not hold for turbulent parts of the ocean (Griffies 2004). Unresolved turbulent flow can indeed impose a significant effect on the main (resolved) flow through non-linear interactions.

In coarse resolution climate- and general circulation models, mesoscale eddies (10-100km) are, in general, part of this unresolved, *sub-grid scale* (SGS) regime. SGS refers to dynamics taking place on spatial and/or temporal scales smaller than the discrete grid of the model. These eddies are shown to be the most energetic component of variability (e.g., Chelton et al., 2007) and a ubiquitous feature of the World Ocean (as confirmed by satellite observations increasing both in number and quality). Therefore it is imperative to consider and addressing these mesoscale/SGS dynamics in ocean climate models and coarse resolution models in general. This is done by *parameterizing* these processes, meaning, describing the net effect of unknown turbulent variables in terms of our resolved variables (also referred to as *upscaling*). To optimally achieve this, however, it is necessary to understand and

interpret eddy fluxes. This has for quite some time been, and still is, a field of intense research.

Historically, a simple down-gradient diffusion with different coefficients in horizontal and vertical directions was used to describe the net effect of the SGS flows and to suppress numerical noise. This was later improved to neutral diffusion (Redi, 1982) before the GM scheme (Gent-McWiliams, 1990) was suggested to describe the previously neglected role of mesocsale eddies that exerts to restratify the ocean by flatting out isopycnals through a process called *stirring* (quasi-adiabatically transporting parcels around and to release available potential energy stored in the baroclinicity the system). Each of these concepts are described and explained in detail in Section 2. The strengths of such isopycnal diffusion and GM stirring are normally governed by the same parameter, κ, in which we also focus on in this study.

One of the many challenges that present themselves in today's ocean modeling research is how to optimally set the size and distribution of this parameter. The original GM paper (1990), stated that the nature of the parameter κ itself was beyond the scope of the manuscript. Over the course of the years, however, many suggestions have been published. Visbeck et al. 1997 was among first to propose a method determining a coefficient that was horizontally varying based on flow dependent diagnostics of expected eddy activity[1]. In our study, the primary objective is to test and compare four different such closure schemes. In that regard, these pages can be considered a follow-up or a supplement to the paper of Eden et al. (2008). Our approach is more direct, however. Where they compared output from a climate model with the climatology of Levitus & Boyer (1994) we aim to diagnose or compare the diffusivity closures directly with processed output from our eddy resolving model. Thus we need not to worry about model based errors (dynamical algorithms, choices of boundary forcings, etc.) or lacking climatology. On the other hand, our study is strictly (and merely) theoretical in nature and also face its own challenges and caveats. How to define and interpret eddy fluxes obtained directly from a high-resolution grid

[1] Similar flow-dependent diffusivities had already been proposed for atmospheric applications by Green (1970) and Stone (1972)

is not a trivial matter. And complications arise because these fluxes contain rotational components that do not affect the tracer equations (due to their non-divergence, that is, they bring in equally much tracer to a region as they remove), but still influence the variables used to compute the eddy diffusivities (e.g., Bryan et al., 1999; Eden et al., 2006). This fact complicates the prospects of capturing physically meaningful results from a direct calculation. These issues have been affronted by many attempts to define (and remove) the rotational fluxes. A Helmholtz-decomposition may be used to separate a (sufficiently smooth) vector field into divergent and rotational parts (e.g., Lau & Wallace, 1979; Roberts & Marshall, 2000). However, such a decomposition depend on the choice of boundary conditions and is consequently not unique (Fox-Kemper et al., 2003). Other studies have assumed the eddy variance equation and associate rotational fluxes with advection of variance (e.g., Marshall & Shutts 1981, Medvedev & Greatbatch 2004). In this study we attempt to utilize the method of Medvedev & Greatbatch (2004, hereafter referred to as MG), in an experiment similar to one earlier demonstrated by Eden et al., (2006), Eden (2007). Additionally, we attempt to sidestep the entire issue with rotational fluxes by considering the divergence of the eddy-diffusivity fluxes directly, compared with the divergence of the parameterization. By construction, the rotational fluxes vanish, but more derivatives may result in excessive noise that may obscure the signal we seek (Nakamura and Chao, 2000; Bryan et al., 1999; Tanaka et al., 2007).

Earlier numerical studies report of little actual correlation between the eddy fluxes and the down-gradient assumption (also appearing in the skew flux formulation of GM, Section 2), an unsatisfactory trait that has generally been ascribed the complications caused by rotational fluxes (e.g, Rix and Willebrand, 1996; Roberts and Marshall, 2000; Griesel et al., 2009). Here we find, with some averaging over many eddy scales (spatial smoothing), a rather clear correlation between the diagnosed eddy fluxes and the mean field gradient (down-gradient parameterization), regardless of rotational fluxes.

In contrast to earlier studies on the topic (of computing diffusivities), almost exclusively done with geopotential coordinate models, we employ a terrain-following model called ROMS (Regional Ocean Modeling System). It is a modern code containing algorithms to minimize the *pressure gradient error* inherent in this branch

of models. Furthermore we use finer resolution (~1/15°) than similar studies, and focus on the Nordic Seas. Our simulation is conducted on a 4000·2000 km domain on a 4 km grid, where bathymetry is included. The solution was integrated over seven years, where the last five years were utilized as analyzation period. No explicit horizontal viscosity/diffusion (other than numerical diffusion from the advection scheme) were needed to keep the solutions stable due to the high resolution. Low viscosity is necessary to retain the characteristics of the small scale flow we seek to define and parameterize. The simulation output data is a courtesy of the Norwegian Meteorological Institute (DNMI).

The transcending goal with this research to expand or support our knowledge about mesoscale eddies, and in particular the magnitude and distribution of the adiabatic stirring and diffusion they evoke, and how this should be implemented into coarse-grid climate models. This aim is motivated by the eddies' fundamental role in transport of tracers (like heat) in the upper water masses of the World Ocean, which may greatly exceed the tracer transport of the mean flow (Isachsen and Nøst, submitted paper) in certain regions[2] and plays a significant role in the heat transport of the meridional overturning circulation. The heat capacity of the ocean is many orders larger than that of the atmosphere and is consequently the controlling factor in respect to long term climate evolution and forecasts. To have a solid understanding of the small scale representation in our ocean models, and in turn how it affects larger scales, becomes of primary importance if we are to obtain climate prognoses that maintain their physical integrity throughout centuries of integration and still yielding output that reflects the true and accurate future evolution of the water masses.

In Section 2 we present the conceptual and mathematical formulations of isopycnal

[2] Particularly in the Southern Ocean, where the mean flow is predominantly zonal and transports little heat poleward.

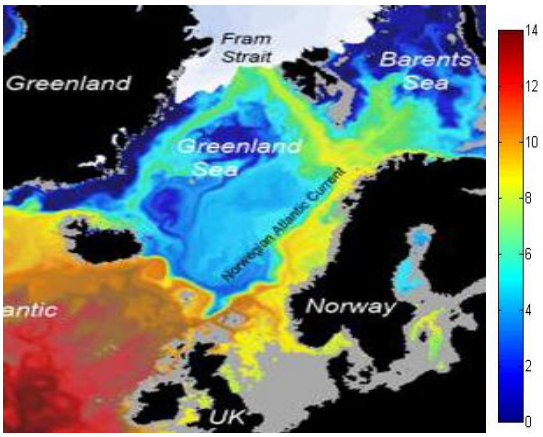

Figure 1.1; Potential temperature (colors) at 100m depth and sea ice (grey/white) distribution in winter 2006, based on an 8 km model. Picture is borrowed from Aksenov et al., (2009).

diffusion and GM stirring operators (first in (i) structure, then in (ii) magnitude). The concepts will be thoroughly explained for completeness and pedagogical value. The practical results we represent are mostly tied to item (ii), so seasoned readers may want to skip or skim through the first sub-Sections. Thereafter we discuss decompositions of fluxes and the method proposed by Medvedev & Greatbatch 2004, hereafter referred to as MG), and introduce the diffusivity closures that are to be evaluated. In Section 3 we discuss the ROMS model (the source model used to produce the output data the upcoming diagnostics are based on) and specifications/ configurations thereof. The various experiment set-ups and results are presented in detail in Section 4. Section 5 contains a final discussion and summaries.

Section 2: Theory

As stated in Section 1, a stochastic approach is necessary because some dynamical scales cannot be resolved by discrete numerical ocean models. These physics must be parameterized, and we present here a common way of describing the *SGS* mathematically. Let ϑ be an arbitrary tracer, which is transported by an advective flux vector $\boldsymbol{F}_{adv} = \boldsymbol{u}\vartheta$ where $\boldsymbol{u}$ is the advective velocity, and a diffusive flux vector $\boldsymbol{F}_{dif}$ representing viscous molecular exchanges given as $\boldsymbol{F}_{dif} = -k_m \boldsymbol{\nabla}\vartheta$, where k_m is a coefficient quantifying the strength of the friction. At an Eulerian point in space it is the divergence (convergence) that decreases (increases) the concentration of tracers.

$$\partial_t \vartheta = -\boldsymbol{\nabla} \cdot (\mathbf{F}_{\mathrm{adv}} + \mathbf{F}_{\mathrm{dif}}) + S \tag{1}$$

Where ∂_t is a shorthand notation for differentiation with respect to time, S is a specific source term affecting tendency which is otherwise irrelevant to the following discussion. The above fluxes also takes place in the momentum equation (assuming a hydrostatic Boussinesq fluid),

$$\partial_t \mathbf{v} = -\boldsymbol{\nabla} \cdot (\boldsymbol{\mathcal{F}}_{\mathrm{adv}} + \boldsymbol{\mathcal{F}}_{\mathrm{dif}}) - \mathrm{f}(\mathrm{k} \times \mathbf{v}) - \frac{\boldsymbol{\nabla} \mathrm{p}}{\rho} \tag{2}$$

Where $\boldsymbol{v} = (u\boldsymbol{i} + v\boldsymbol{j} + w\boldsymbol{k})$, f the coriolis parameter and p the in situ pressure. Special characters denotes tensors, since $\boldsymbol{\mathcal{F}}^{\boldsymbol{v}}{}_{dif} = -k\nabla\boldsymbol{v}$

The $\boldsymbol{F}_{dif}$ and $\boldsymbol{\mathcal{F}}_{dif}$ molecular diffusive fluxes appearing in these equations usually take on an additional role as discussed next (diffusive flux is commonly referred to as viscosity or kinematic viscosity in association with momentum).

2.1 Diffusion as sub-grid scale closure

Consider a two-dimensional standard numerical A-grid of equal spatial resolution. The value of the tracer, momentum or density obtained in one of these grid boxes must represent an average value of the tracer taken over the entire spatial square A, equaling Δx times Δy, as illustrated in Figure 1 Regarding time as a third dimension, we get the average of a space-time 'box', so that

$$\overline{\vartheta} = \frac{1}{\Delta A \Delta t} \int_{-\Delta t/2}^{\Delta t/2} \int_{-\Delta A/2}^{\Delta A/2} \vartheta \, dA dt \tag{3}$$

These averaged values inevitably brings with them information loss about sub-grid of the system we attempt to simulate. This problem becomes less dominant with higher resolution (smaller values of delta A and delta t), but a satisfactory resolution in this sense is unrealistic even for a limited area ocean model. Even then, numerical models on a discrete lattice, regardless of the resolution, may not be loyal to dynamics based on a continuum hypothesis.

The *averaged* advective flux $\overline{\boldsymbol{F}_{adv}} = \overline{\boldsymbol{v}\vartheta}$ then appearing in the governing tracer equation (and momentum equations) may, through Reynolds averaging, be decomposed into means and deviations from the mean. Striking out averages of deviations, we obtain the expression

$$\overline{\mathbf{v}\vartheta} = \bar{\mathbf{v}}\bar{\vartheta} + \overline{\mathbf{v}'\vartheta'} \tag{4}$$

This introduces a new term to the (averaged) tracer equation so that,

$$\partial_t \bar{\vartheta} + \boldsymbol{\nabla} \cdot \left(\bar{\mathbf{v}}\bar{\vartheta}\right) = -\boldsymbol{\nabla} \cdot \overline{(\mathbf{v}'\vartheta')} + \mathrm{k_m}\boldsymbol{\nabla}\bar{\vartheta} \tag{5}$$

The variable $\overline{\boldsymbol{v}}$ (and $\bar{\vartheta}$ as appearing in (5)) can be interpreted as the flow explicitly resolved and described by our model, and is the basis for the *mean* flow depicted in Figure 1. In contrast, the inconvenient correlation-term $\overline{\boldsymbol{v}'\vartheta'}$ is a vector of turbulent variables that we have no explicit knowledge of, and may be interpreted as turbulent eddy activity. Still, it describes important sub-grid scale processes with non-trivial effect on the mean flow.

To parameterize, or *upscale,* this effect, we must describe it in terms of our resolved

variables (i.e., a stochastic approach as mentioned in Section 1). Figure 1.1 abstractly illustrates the unresolved turbulent movement that happens in between our finite discrete lattice.

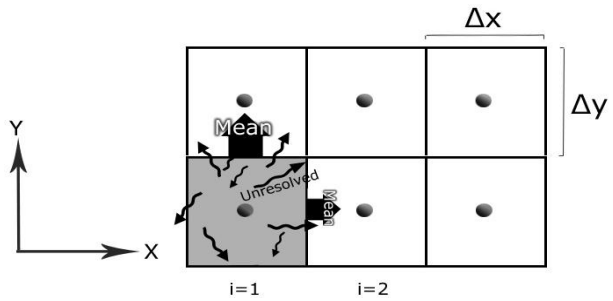

Figure 2.1; Abstract illustration of a typical two-dimensional A-grid. Dots represents the exact position of the known variables, spaced Δx and Δy apart. The point value of variables, like tracers and momentum, must be interpreted to be the average within the containing square. That is, all we know is the mean of the grey scaled area, as exemplified in the lower left square. As a result, we only have information of the mean flow depicted as thick arrows, but cannot explicitly describe the smaller flow (depicted as curly random arrows).

Theories of turbulence often start with analogies to movement of random walk particles (Reif, 1965) advecting tracers and momentum around arbitrarily. This means that even though the mean of all the displaced distances will always be close to and eventually converge to zero, the *root-mean-square* of the distances will increase by a factor proportional to the square root of time (Vallis, 2005). From an averaged perspective a huge number of particles, or advections, will statistically behave predictably (that is, a manner easy to describe mathematically), as tracers will be transported from regions of high to low concentration and thus manifest in the form of *down-gradient diffusion*. These are well tested ideas from statistical physics (Griffies, 2004).

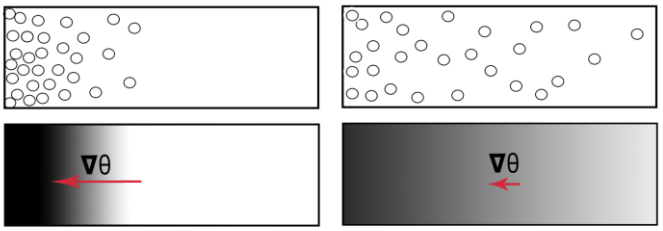

Figure 2.2; Random movement of particles (or small scale advection) at a time T (left hand pane) and a later time T+ΔT (right hand pane). Considering a myriad of random walk particles (bottom pane) statistically removes all randomness from the system. Tracers are carried from areas of high concentration to areas of low concentration, a process called downgradient diffusion. This means a flux with magnitude oppositely proportional to the well-defined gradient vector (which in this simplified case is $-\partial_x \vartheta$*).*

These conclusions lead to

$$\mathbf{F}_{\mathrm{SGS}} = -\mathrm{k}\,\partial_{\mathrm{x}}\vartheta = \overline{\mathrm{u}'\vartheta'} \tag{6}$$

or in the three-dimensional case,

$$\mathbf{F}_{\mathrm{SGS}} = \overline{\mathbf{v}'\vartheta'} = -\mathrm{k}\boldsymbol{\nabla}\vartheta \tag{7}$$

Where the $\boldsymbol{\nabla}$-operator is the sum of derivatives in all three dimensions, and the coefficient k describes the efficiency of the diffusion process.

This type of parameterization, commonly seen in association with theories of molecular diffusion of temperature (e.g., Fick 1855) in thermodynamics (illustrated by Figure 2.2), is totally analogous with the theory of SGS physics. Because of the mathematical and structural similarities (between fluxes $\boldsymbol{F}_{dif}$ and $\boldsymbol{F}_{SGS}$), these different regimes of physics may be combined into a common diffusion operator accounting for both. The diffusion arising from the turbulent advective transport is far prevalent over the molecular viscous exchanges, however. Grids must be refined to the Kolmogorov scale (a few millimeters) for these effects to have identical order of magnitude (Griffies, 2004). Therefore, the molecular contribution is simply absorbed into the $\boldsymbol{F}_{SGS}$ term. For this reason such downgradient SGS closures is referred to as *enhanced diffusion.*

Papanicolaou and Pironneau (1981) showed that the analogy between the molecular diffusion and eddy diffusivity holds as long as there is a significantly large separation between the spatial and temporal scales of the eddies and the large-scale circulation, which is what we assume in ocean dynamics.

It should be noted that this diffusion can be, in addition to a reasonable physical assumption, interpreted simply as a numerical necessity to suppress growth of variance in the solutions. With insufficient diffusion incorporated into the system, energy will cascade to smaller scales and ultimately pile up at grid scale (smallest 'available' scale in the numerical system) increasing variance to unphysical levels. This is commonly referred to as numerical noise, something which may quickly lead to instability, even for implicitly timed models or models otherwise satisfying the CFL-condition (Røed, 2009). The diffusion or viscosity needs to dissipate this variance increase by smoothing out the fields. Numerical noise may in turn be

explained solely by the deficient information exchange between grid points, in a system originally formulated as a continuum. So the two interpretations could very well be two sides of the same coin. Nonetheless, we emphasize on the description of diffusion as averaged physics rather than solely as a happen-to-be numerical necessity.

2.2 Structure of the parameterizations (i).

When *upscaling* or employing a parameterization of the sub-grid scale processes, there are two main issues to consider.

(i) The structure and form of the mixing processes, or *"how it works"*.

(ii) The magnitude of the mixing, e.g., as a function of the mean flow, or *"when (and how much) it works".*

We will consider item (i) in this section and item (ii) in Section 2.3. The practical results of this study are mainly tied to (ii). However, we will also discuss item (i) for completeness. After all, it is an essential theoretical fundament for understanding the role of eddies and the parameter (κ) we seek in (ii).

2.2.1 Anisotropic diffusion

While the smallest micro scale turbulence and mixing may be well approximated by equation (7), transport at mesoscale and larger exhibits a substantial amount of anisotropy (Griffies, 2004), where mixing processes in the horizontal is far more effective than vertical processes. This is due to the density stratification in the inner ocean. If a parcel is lifted (or depressed) from its resting position in a fully barotropic ocean with no horizontal density gradient, it will become less (or more) buoyant than its surroundings and be subject to a restoring force. In contrast, no such restoring force will appear when the parcel is shifted horizontally. Less resistance implies that more

effective mixing will happen in this direction. This prescribes the need to adjust the diffusion coefficient k to a parameter different in the vertical (v) than in the horizontal (h). It is then formulated as,

$$\mathbf{F}_{\mathrm{SGS}} = \overline{\mathbf{v}'\vartheta'} = -\boldsymbol{\mathcal{K}} \cdot \boldsymbol{\nabla}\vartheta \tag{8}$$

where $$\boldsymbol{\mathcal{K}} = \begin{bmatrix} h & 0 & 0 \\ 0 & h & 0 \\ 0 & 0 & v \end{bmatrix}$$

Inserting (8) into the tracer equation (5), we arrive at the following expression.

$$\partial_t \overline{\vartheta} + \nabla \cdot \left(\overline{\boldsymbol{v}}\overline{\vartheta}\right) = -\nabla \cdot \overline{(\boldsymbol{v}'\vartheta')} = \nabla \cdot (\boldsymbol{\mathcal{K}} \cdot \nabla\vartheta) \tag{9}$$

This kind of mixing was used throughout the 1970's until George Veronis pointed out a contributory reason for the inadequate simulation results of the Meridional Overturning Circulation in the Atlantic (as well as large unphysical downwellings) obtained at the time, and explained in a paper (Veronis, 1975) what was to be called the *Veronis effect*. The problem was established to be that the large horizontal diffusion contained an unacceptable amount of *diapycnal diffusion*.

2.2.2 Isopycnal / neutral diffusion

Consider the same basin as before, but include a significant amount of baroclinicity (tilting surfaces of constant *potential* density). If a parcel existing on one of these surfaces now is moved purely horizontally, the parcel will now be more buoyant than its surroundings and being forced upwards towards the density-surface it was originally resting on. The result of this is that turbulent mixing happens more effectively along isopycnals (Iselin, 1939). Or more specifically, but subtly, along Neutral surfaces (McDougall, 1987). (If the process is fully adiabatic, the parcel will stick to its isopycnal). This is also often referred to as *lateral* in the literature. It is however clear that the pure horizontal mixing used in models were ruthlessly crossing the relevant stratification. So to remedy this problem, it was suggested the diffusion tensor $\boldsymbol{\mathcal{K}}$ must describe not vertical and horizontal, but instead isopycnal (I) and

diapycnal (D) diffusion. That is,

$$\mathcal{K}_{NEUTRAL} = \begin{bmatrix} I & 0 & 0 \\ 0 & I & 0 \\ 0 & 0 & D \end{bmatrix} = I \begin{bmatrix} 1 & 0 & 0 \\ 0 & 1 & 0 \\ 0 & 0 & \epsilon \end{bmatrix} \tag{10}$$

Where ϵ is the ratio between the diffusivities in the orthogonal directions, usually a very small number. This must be described in a set of *local orthonormal coordinates*, where two unit vectors are spanning out the density surface (locally) and the third is orthogonal and normal to the surface. The unit vectors become,

$$\hat{\mathbf{e}}_1 = \frac{\nabla\rho}{|\nabla\rho|} \ , \qquad \hat{\mathbf{e}}_2 = \frac{\mathbf{j}\times\nabla\rho}{\mathbf{j}\times|\nabla\rho|} \ , \qquad \hat{\mathbf{e}}_3 = \hat{\mathbf{e}}_1 \times \hat{\mathbf{e}}_2$$

And the Slope-vector **S**, defined by the ratio between the horizontal gradient and the vertical gradient,

$$\mathbf{S} = (S_x, S_y) = \nabla_\rho z = -\frac{\nabla_H \rho}{\partial_z \rho} \tag{11}$$

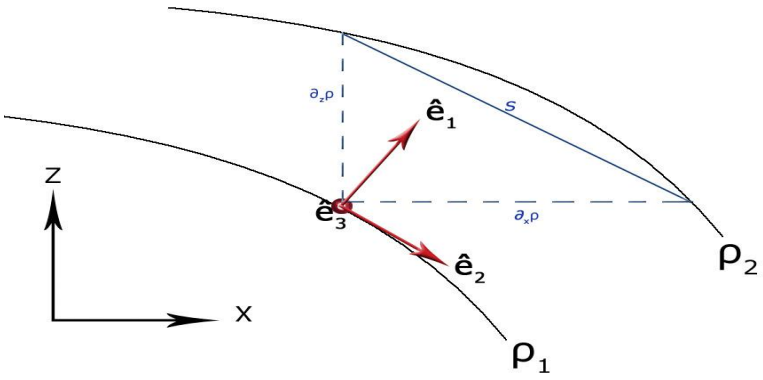

Figure 2.3; Schematic of two density surfaces ρ and $\rho+\Delta\rho$ and the basis vectors of the local orthonormal coordinates. The slope-vector is shown in blue. Note that the curvature is much exaggerated compared to most of the ocean, but isopycnals may take such a form near boundaries or convective areas, in which case the Small Slope Approximation breaks down.

where ρ rho is the density of the water. A coordinate system with shifting axes is highly inconvenient base for a dynamical ocean model, so the new diffusion tensor $\mathcal{K}_{NEUTRAL}$ must be rotated from the orthonormal coordinates to the coordinate system

of the model, as derived by Redi (1982). We still assume geopotential coordinates here, but a similar process for terrain-following coordinates can be found in Røed, (2001). Following Redi (1982), we obtain,

$$\boldsymbol{\mathcal{K}}_{REDI} = \mathrm{I}\begin{bmatrix} 1+\boldsymbol{S^2} & S_xS_y & S_x \\ S_xS_y & 1+S_yS_x & S_y \\ S_x & S_y & \epsilon+|\boldsymbol{S}|^2 \end{bmatrix} \tag{12}$$

It is immediately apparent that the new diffusion tensor $\boldsymbol{\mathcal{K}}_{REDI}$ is more complicated and contains off-diagonal terms. Fortunately, with the knowledge that isopycnal slopes in the interior ocean usually are much less than 1/100, we may assume $\boldsymbol{S}$ to be very small, so terms including factor $\boldsymbol{S^2}$ may be neglected in the diffusivity tensor. This is called the *small slope approximation*. We then arrive at,

$$\boldsymbol{\mathcal{K}}_{REDI} = \mathrm{I}\begin{bmatrix} 1 & 0 & S_x \\ 0 & 1 & S_y \\ S_x & S_y & \epsilon+|\boldsymbol{S}|^2 \end{bmatrix} \tag{13}$$

It should be noted that the Small Slope Approximation breaks down in turbulent domains such as boundary layers or convective areas where the isopycnals may climb rather steeply, if not entirely vertical.

Using the new three-dimensional diffusion tensor, we may calculate the isopycnal diffusive flux vector appearing in equation (8), (9).

$$\begin{gathered} \mathbf{F}_{\mathrm{SGS\,ISO}} = -\boldsymbol{\mathcal{K}} \cdot \boldsymbol{\nabla}\vartheta = \\ -\mathrm{I}[(\boldsymbol{\nabla}_{\mathrm{H}}\vartheta + \mathbf{S}\,\partial_{\mathbf{z}}\vartheta)] - \mathrm{I}[\mathbf{S} \cdot \boldsymbol{\nabla}_{\mathrm{H}}\vartheta + (\epsilon + \mathbf{S^2})\,\partial_{\mathbf{z}}\vartheta]\mathbf{k} \end{gathered} \tag{14}$$

Fluxes may be decomposed into a down-gradient component, associated with a symmetrical transport tensor $\boldsymbol{S}$, and an along-gradient component, associated with an anti-symmetric transport tensor denoted $\boldsymbol{A}$, so that,

$$\boldsymbol{S} = \frac{1}{2}(\boldsymbol{\mathcal{K}} + \boldsymbol{\mathcal{K}}^T) \quad , \tag{15}$$

$$\boldsymbol{A} = \frac{1}{2}(\boldsymbol{\mathcal{K}} - \boldsymbol{\mathcal{K}}^T) \ ,$$

where $\boldsymbol{\mathcal{K}}^T$ denotes the transpose of the tensor. So far $\boldsymbol{\mathcal{K}}$ has simply been a symmetric matrix describing downgradient diffusion, that is, until now $\boldsymbol{\mathcal{K}} = \boldsymbol{S}$. The very different physical property[3] of the anti-symmetric tensor $\boldsymbol{A}$ and its advective utility will be discussed next.

2.2.3 The Gent-McWilliams Stirring Operator

The GM *stirring* scheme parameterizing the effects of unresolved mesoscale eddies published by Gent-McWilliams in 1990 was rather revolutionary within the field of ocean climate modeling. The idea originated when Gent and Cane worked on a tropical model investigating El Ninõ effects during the late 80's (Gent, 2011). They made the approximation ρ=ρ(T) for the equation of state for seawater, ignoring density changes due to pressure and salinity. This was a reasonable approximation, because the non-linear equation of state is greatly dominated by temperature changes in warm waters of the tropics. When about to implement the well-established theory that mesoscale eddies mix tracers predominantly in neutral directions, they soon realized that it would have no effect; isolines of potential temperature would now coincide with that of potential density surfaces, and temperature cannot be diffused along lines of constant temperature. Seemingly something were lacking in the parameterization of mesoscale eddies, as they had no effect under these highly reasonable assumptions. Gent and McWilliams constructed a parameterization to compliment the isopycnal Redi-diffusion, called *stirring*, which reversibly and adiabatically rearranges fluid parcels around adiabatically (naturally) as defined by an anti-symmetric transport tensor.

The GM scheme was based on the postulates that,

1) *Moments of the tracer (amount and variance) should be conserved, and buoyancy should not diffuse across its isolines.*
2) *The stirring should release APE from the system, akin to baroclinic instability.*

[3] Keep in mind that diffusive processes dissipate variance whereas advective processes conserve variance.

The latter postulate is satisfied if the stirring coefficients increase with the slope of the isopycnals. Gent et al. (1995) formulated a simple anti-symmetric transport tensor,

$$\mathbf{A} = \kappa \begin{bmatrix} 0 & 0 & -S_x \\ 0 & 0 & -S_y \\ S_x & S_y & 0 \end{bmatrix}, \tag{16}$$

Where the coefficient κ determines the strength of the reversible mixing. An associated stream function is found by,

$$\psi = (-\kappa S_y, \kappa S_x, 0) \tag{17}$$

Because ψ is a stream function, its curl, $\boldsymbol{\nabla} \times \psi$, yields the corresponding velocities,

$$\mathbf{u}^* = -\partial_z(\kappa \mathbf{S}) \quad , \quad w^* = -\nabla_H(\kappa \mathbf{S}) \tag{18}$$

where κ is a stirring coefficient (note that this coefficient is sometimes referred to as *thickness diffusivity,* which is otherwise only the same under certain conditions.[4]

S is the slope-vector as defined in Section 2.2.1. In words, this means that a local increase of the slope, resulting in a horizontal variation of density and thus a center of mass higher than equilibrium, will cause movement (an advection) to re-level this center of mass, as illustrated in Figure 4.

According to Gent et al. (1995), it is the residual velocity, the sum of the resolved velocity $\bar{\boldsymbol{u}}$ and the extra eddy induced velocity $\boldsymbol{u}^*$ that advects *all* the tracers in the governing equations of the model.

$$\partial_t \bar{\vartheta} + \nabla \cdot ([\bar{\mathbf{v}} + \mathbf{v}^*]\vartheta) = -\nabla \cdot (\boldsymbol{\mathcal{K}} \cdot \nabla \vartheta) \tag{19}$$

[4]Principally in cases of flat bathymetry. GM stirring will flatten out isopycnals in the horizontal.

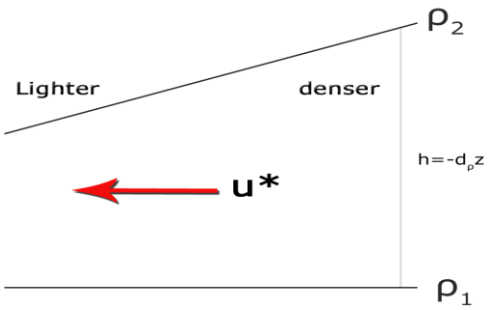

Figure 2.4; Vertical variation in thickness h. Eddies stir up and restratify the system by establishing an extra advection of magnitude $\mathbf{u}^* = -\partial_z(\kappa \mathbf{S})$. *If the lower ρ-surface is tilted less than the upper, this is equivalent to thickness diffusion.*

As an alternative to this advection, Griffies (1998) suggested that this flux instead being described as a skew flux, or *skewsion*. Consider the eddy advective flux caused by an extra eddy induced three dimensional velocity $\boldsymbol{v}^*$. This non-divergent velocity may be described through any stream function that satisfy $\boldsymbol{v}^* = \boldsymbol{\nabla} \times \boldsymbol{\psi}$. Simple vector algebra can reform this expression to terms,

$$\begin{aligned} \mathbf{F}_a = \mathbf{v}^* \vartheta &= (\boldsymbol{\nabla} \times \boldsymbol{\psi})\vartheta \\ &= \underbrace{\nabla \times (\boldsymbol{\psi}\vartheta)}_{\text{ROTATIONAL}} - \underbrace{\boldsymbol{\nabla}\vartheta \times \boldsymbol{\psi}}_{\text{SKEW}} \end{aligned} \tag{20}$$

The terms on the right hand side are known as the rotational flux and the skew flux, respectively. Since the rotational flux is non-divergent because $\boldsymbol{\nabla} \cdot \boldsymbol{\nabla} \times (\boldsymbol{\psi}\vartheta) = 0$, the divergences of the skew flux and the advective flux must be identical. This means that one may use either divergence to describe the evolution of tracers. The former is downgradient whereas the latter is across-gradient (along isolines, Figure 2.5). The along obvious because $\nabla\vartheta \cdot \boldsymbol{F_{skew}} = \nabla\vartheta \cdot (\nabla\vartheta \times \boldsymbol{\psi}) = 0$. The skew flux thereby conserves variance, a trait shared by advection. Inserting the stream function (17) into the skew flux $\boldsymbol{F_{skew}} = (\nabla\vartheta \times \boldsymbol{\psi})$ and decomposing, we arrive at

$$\begin{aligned} \mathbf{F}_{\text{skew}} = -\boldsymbol{\nabla}\vartheta \times \boldsymbol{\psi} = -\begin{pmatrix} \mathbf{i} & \mathbf{j} & \mathbf{k} \\ \partial_x\vartheta & \partial_y\vartheta & \partial_z\vartheta \\ -\kappa S_y & \kappa S_x & 0 \end{pmatrix} = \\ \partial_z\vartheta\, \kappa\, \mathbf{S} + \kappa(\nabla_{\mathbf{H}}\vartheta \cdot \mathbf{S})\mathbf{k} \end{aligned} \tag{21}$$

Note that if $\boldsymbol{\vartheta}$ are taken to be potential density (or parallel to potential density), we may use (11) to eliminate the slope in the horizontal terms and find,

$$\begin{aligned} \mathbf{F}^{\mathrm{H}}_{\mathrm{skew}} &= -\kappa \boldsymbol{\nabla}_{\mathrm{H}} \rho \;=\; \overline{\mathrm{u}'\rho'}\mathbf{i} + \overline{\mathrm{v}'\rho'}\mathbf{j} \\ \mathrm{F}^{\mathrm{V}}_{\mathrm{skew}} &= -\kappa(\boldsymbol{\nabla}_{\mathrm{H}} \rho \cdot \mathbf{S}) \;=\; \overline{\mathrm{w}'\rho'}\mathbf{k} \end{aligned} \tag{22}$$

Eq. (22) is central to this study. It is evident that the *horizontal* part of the GM skew flux acts as a simple Fickian diffusion down the *horizontal* gradient of ϑ.
For an arbitrary tracer, total transport flux is now given by the sum of the symmetrical and anti-symmetrical SGS transport components, the Redi-flux (14) and the GM skew flux (22) respectively. The total SGS mixing flux then becomes,

$$\begin{aligned} \mathbf{F}_{\mathrm{SGS}} = \; & \partial_{\mathbf{z}}\vartheta(\kappa - \mathrm{I})\mathbf{S} - \mathrm{I}\boldsymbol{\nabla}_{\mathrm{H}}\vartheta - \mathbf{k}[(\kappa + \mathrm{I})\mathbf{S} \cdot \boldsymbol{\nabla}_{\mathrm{H}}\vartheta \\ & + \kappa(\epsilon + \mathrm{S}^2)\,\partial_{\mathrm{z}}\vartheta] \end{aligned} \tag{23}$$

It should be noted that when stirring is identical to isopycnal diffusion, that is, $\kappa = \mathrm{I}$, the horizontal component reduces to a normal horizontal diffusion. This is a kinematic result that arrives from the exact cancellation of off-diagonal terms in the two mixing tensors $\boldsymbol{S}$ and $\boldsymbol{A}$. Griffies (1998) points out that computing both processes (using the skew flux formulation) is numerically cheaper than computing each on its own, given that $\kappa = \mathrm{I}$. This common choice of identical isopycnal diffusion and eddy stirring strengths is mostly based on simplicity and convenience. However, Smith and Dukowhich (1997) provide arguments suggesting that this may also be physically reasonable.

Despite the horizontal simplification granted by the skew flux approach, the more complicated vertical flux is a crucial piece of the GM parameterization to include in coarse resolution models to respect the underlying (quasi adiabatic) physical properties.

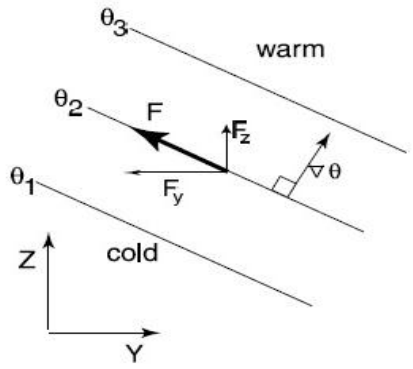

Figure 2.5; GM skew fluxes as seen in a zonal mean, arising from sloping isopycnals. The skew flux itself is neither upgradient or downgradient, but its horizotal component directed downgradient whereas the vertical component is upgradient5. The role of this upgradient flux is to lower the center of gravity (i.e., release APE).

Eden et al. (2007) argues that the horizontal part of the skew flux, which is diffusive in character (parameter κ), should in turn have a *skew* counter-part that acts as an advection in the horizontal plane (parameter ν). The rationale was based on the appearance of prominent along-isopycnal eddy fluxes in regions of dominating mean flow, suggesting that an isotropic parameter is insufficient. Despite their emphasis on the relevance of this previously neglected part of the GM-parameterization, they do not seem to maintain the importance in a later paper (Eden, 2010). Simulations of energetic eddy-driven zonal jets showed that the physically relevant diffusivity indeed were predominantly downgradient and thus appropriate for isotropic stirring[6] (i.e., single stirring parameter).

To intuitively visualize the difference between the diffusive flux parameterization (the symmetric part) and the adiabatic stirring, i.e. the pseudo-advective skew flux (the anti-symmetric part), imagine a bowl of water with drops of dense concentration of red dye poured into the middle. If the mixing process were exclusively (fickian) diffusive in three dimensions, the dye would expand in a sphere turning pink as the red color thinned out. Meaning, the amount of dye in each parcel would even out, changing the properties of each parcel. On the other hand, if the mixing were exclusively a stirring, the parcels would keep their properties but would be rearranged

[5] An upgradient (vertical) diffusion is unproblematic in terms of numerical stability as long as the net flux is not upgradient (Griffies, 1998).
[6] Note that the isotropy applies only to the horizontal component of the GM skew fluxes. The process is in general adiabatic, i.e., along neutral surfaces (local isopycnal surfaces).

and stretched into finer filaments; the dye would spread into thin swirls and streaks of red, but would not diffuse to pink. In principle, this result of the stirring could be reversed by advecting the parcels back to the original distribution[7] and is therefore called a *reversible* process. The former (diffusive) process is *irreversible* as the dye cannot be "un-diffused" back into its original parcels or concentration.

2.3 Magnitude of the parameterizations (ii)

What is the effective strength of the eddy stirring processes? The original GM (1990) paper made no attempt to determine the magnitude or distribution of the coefficient κ, taking it to be a topic of future research. And it still is, over 20 years later. Most climate models run in the first decade after GM's inception used constant values of diffusivities $\kappa = I \sim 1000\, m^2/s$, as suggested as a rough approximation in the original GM (1990) paper.

Visbeck et al. (1997) was among the first to suggest a flow dependent closure for the strength of the GM stirring parameter. The general idea was, as earlier seen in meteorology, to express the mixing coefficient in terms of an appropriate time and squared length scale (the units of diffusivity). It could be evaluated as,

$$\kappa \sim \frac{L^2}{T} \qquad or \qquad \kappa \sim L\, v' \sim L\bar{v} \ , \tag{24}$$

approximating the eddy velocity to that of the mean flow. Here L is a typical eddy length scale and T is a characteristic eddy time scale. If we suppose that eddies are generated by baroclinic instability, it is natural to compare the mixing length to the Rossby radius of deformation, $L_r$or length of the baroclinic zone, L_z. The time scale would be associated with the growth rate of waves in Eady instability theory, i.e., the ratio of the Richardson number (a measure of baroclinic instability) and coriolis parameter. In coherence with instability theories (e.g., Eady 1949) , the early closures were depth-independent. However, observations affirm that eddy activity decreases

[7] This can be shown in laboratory experiments with rotating laminar flow fluids.

with depth, and some closures respect this fact.

There is a principal fact that diffusivities must be scaled with grid size; refining the grid requires reduction of SGS diffusivities (Section 2.1). But quite adversely, for refined grids, the Eady growth rate (eddy time scale, see 2.3.1) and in turn the diffusivity, rather *increases* because the model allows for more vigorous mean flows and stronger gradients (Griffies, 2004), normally causing closures to over-diagnose diffusivities. Therefore the model's local grid size, Δ, should also be considered in the proposed eddy length scale.

Coarse resolution models depend on a proper closure for the diffusivity parameters. If diffusivity variations depend only on space (i.e., approximately stationary regions of eddy activity), it would be possible to compute the spatial distribution in advance with a high resolution analogue and use this information in the climate model. If, however, diffusivities also are a significantly changing function of time (as usually assumed), adjusting with the current resolved flow, the diagnosis of κ would have to depend entirely on the schemes based on the large scale flow information available in these models. Inconveniently, coarse resolution models of long integration times are quite sensitive to their SGS parameterizations (e.g., Griffies 2004). So formulating and validating these closures are of utmost importance. We follow here the 2008 paper of Eden, Jochum and Danabasoglu (Eden et al., hereafter ED08)

2.3.1 Visbeck et al. (1997), "VMHS".

In the closure of Visbeck et al., hereafter VMHS, the eddy diffusivity is given by

$$\kappa = \alpha L^2 \bar{\sigma} \,, \tag{25}$$

the right hand side being, respectively, a simple tuning parameter, the length scale and an inverse time scale. The time scale $\bar{\sigma}$ is given as the mean Eady growth rate (depth averaged within the mean thermocline of the ocean),

$$\bar{\sigma} = \frac{\overline{f}}{\sqrt{Ri}} \tag{26}$$

and the overbar represent a vertical mean. Ri is the Richardson number,

$$Ri = \frac{N^2}{|\partial_z \boldsymbol{u}|^2} \ , \tag{27}$$

that is the ratio of density stratification (buoyancy or Brunt-Vaisala frequency) to vertical velocity shear, which measures the growth potential of baroclinic instabilities (e.g., Kelvin-Helmholtz instability). When this number is small, the vertical shear has enough energy to extract potential energy from the stratification (Griffies, 2004). The eddy length scale were proposed to be used as the maximum of the local Rossby radius of deformation L_r, the local grid spacing of the model Δ, and the width of the baroclinic zone L_{bz}. In agreement with Eden et al. (2008), we dropped the last parameter because it is troublesome to quantify precisely. The length scale is then normally given by $L = \max(\Delta, \bar{L}_r)$, but we instead found it advantageous to use,

$$L = \frac{2\,\Delta\,L_r}{\Delta + L_r} \qquad \text{where} \qquad \Delta = \frac{2\,\Delta x\,\Delta y}{\Delta x + \Delta y} \tag{28}$$

As proposed by e.g., Griffies (2004). This makes for a length scale transition ensuring that both parameters always influences L, which normally is not the case in models or domains where $\Delta >> L_r$ and $\Delta << L_r$.

The averaged baroclinic Rossby radius of deformation is approximated by,

$$\bar{L}_r = \frac{\bar{N} H}{f} \tag{29}$$

Where H is the same averaging height as in (26), Since the value of N was known at every level, the Rossby radius could more precisely be expressed as[8],

[8] Usually, the integration depth, H_{vis}, is taken no longer than 2000 m,. As a rough approximation, we ignored the lowermost s-levels where the depth exceeded this level (mainly in the deep basins). Results showed little sensitivity to this, however.

$$\bar{L}_r = \frac{1}{f} \int_{-H_{vis}}^{0} N \, dz \tag{30}$$

Although irrelevant at high latitudes (and thus our domain), note in passing that a substitute value is needed is needed for f near equator, where the Rossby radius will approach infinity. It is suggested in the closure to use $\sqrt{2\beta c_r}$, were c_r is the baroclinic wave speed. This still appeared to produce unphysically large diffusivities near equator as implemented in the experiments ED08.

2.3.2 Ferreira et al. (2005), "NSQR".

To respect the substantial vertical dependence of observed eddy kinetic energies, Ferreira (2005; implemented by Danabasoglu and Marshall, 2007) proposed making κ proportional to the Brunt-Vaisala frequency squared, so that

$$\kappa = \kappa_0 \frac{N^2}{N_{ref}^2} \tag{31}$$

κ is finally bounded by $\frac{\kappa_0}{10} \leq \kappa \leq \kappa_0$, κ_0 being a base value that is chosen, suggested by Danabasoglu and Marshall (2007) to be 4000 $^{m^2}/_{s}$. N is the local buoyancy frequency,

$$N^2 = -\frac{g}{\rho_0} \frac{\partial \rho}{\partial z}, \tag{32}$$

P is potential density and N_{ref} is defined as value of N found in the uppermost level of the pycnocline, defined locally at each horizontal position. Determining a rigorous value of N_{ref} could pose a challenge, however.

We note that the upper pycnocline and transition to the diabatic mixed layer is unsatisfactory described in certain regions of our model generally showing a

pycnocline reaching the surface, resulting in a vanishing mixed layer. We approximated N_{ref} as the greatest value of N in each column of water (which would normally coincide with the middle of the pycnocline). This automatically ensures that the diffusivity does not exceed κ_0, as otherwise required in the closure. We chose to ignore the lower threshold of κ as diffusivities are expected to take values much lower than 400 $m^2/_s$ in many places based on preliminary tests. Note that this closure is designed to obtain a convenient and well working decay-scale, rather than being a vigorous theoretical result.

2.3.3 Eden & Greatbatch. (2008), "EG".

The closure suggested by Eden and Greatbatch (2008), hereafter EG, is similar to VMHS in that it is based on a theoretical eddy length and time scale,

$$\kappa = cL^2\sigma\,, \tag{33}$$

where c is a tuning parameter and

$$\sigma = \frac{f}{\sqrt{Ri}} \tag{34}$$

The main difference from VMHS is the use of *local* values instead of depth averages and thereby respect the depth dependence of eddy energies. L is given as the *minimum* of the Rossby radius and the Rhines scale $L_{Rhines} = \sqrt{\frac{\sqrt{EKE}}{\beta}}$ with EKE being the eddy kinetic energy. However, we ignored the Rhines scale because it becomes large at higher latitudes. Instead we found it pressing to respect the grid scale. Eventually the same length scale as with VMHS (28) was used, but with the local Rossby radius of deformation given as,

$$L_r = \frac{1}{f} \int_{-H}^{0} \frac{N}{\pi} \, dz \ , \tag{35}$$

following Chelton et al. (1998), where H is the total depth at each horizontal position. In our high latitude domain and with the assumptions made, VHMS and EG can be expected to produce similar results, disregarding depth dependency.

2.3.4 VMHS/NSQR

With the widely used VMHS closure being only horizontally varying and the NSQR closure only (locally) depth dependent, we look into combining them to make an alternative closure. This involves modifying the VMHS by giving it a depth dependency identical to the decaying profile of NSQR. This is simply done by using the values from VMHS instead of the κ_0 appearing in NSQR, eq. (31). When at the same time doubling the tuning parameter α to obtain sufficient mixing strength in the upper water masses decaying with depth, one should obtain values and distributions in rough compliance with the other closures and previous estimates based on both theoretical and observational data[9].

Eden et al. (2008) tested the three of the above closures in a model by comparing long term solutions with the climatology of Levitus & Boyer (1994). In general, this comparison and evaluation is burdened by the lack of large-scale coverage of observational measurements and estimates of eddy statistics. Also, one must consider how the dynamical algorithms and boundary forcing chosen in their CCSM model influence the result and affect the interpretation of the diffusivity closures. For instance, one cannot off-handedly exclude the possibility that "two wrongs make a right" in indirect experiments. Therefore, as a supplementary experiment, we attempt here a simple and direct comparison of the above diagnosis to our calculation of the diffusivities based on the output of an eddy resolving model in a more limited domain.

[9] While previous studies have only been partially successful in diagnosing the gross magnitude of the diffusivities, gathered observational data indicate that eddy energy levels decrease with depth (Gent, 2010).

Hopefully our findings will support or strengthen the verdict of ED08.

2.4 Direct diagnostics and the complications of rotational fluxes

Using output data from an eddy-resolving model, one may in principle quantify the amount of diffusivity (associated with mesoscale eddies) directly. Knowing the correlation term, the horizontal part of equation (22) can be manipulated and solved for κ. Considering eddy fluxes of potential density, it is assessed that

$$\kappa = -\frac{\overline{\mathbf{u}'\rho'}\cdot\boldsymbol{\nabla}_{\mathrm{H}}\bar{\rho}}{|\boldsymbol{\nabla}_{\mathrm{H}}\rho|^2}$$

$$\nu = -\frac{\overline{\mathbf{u}'\rho'}\cdot(\mathbf{k}\times\boldsymbol{\nabla}_{\mathrm{H}}\bar{\rho})}{|\boldsymbol{\nabla}_{\mathrm{H}}\rho|^2} \qquad (36)$$

So that κ describes the amount of mixing transporting density down the horizontal gradients whereas the advective v is across (also in the horizontal). In words, eq. (36) says that the stirring parameter is proportional to the size of eddy fluxes projected onto the mean negative density gradient. (Note that while the vertical contribution is important to consider in ocean models, κ can be solved here considering only the horizontal eddy flux, which is about an order of magnitude larger than the vertical.)
Previous studies (e.g., Rix & Willebrand, 1996; Roberts and Marshall, 2000; Eden et al., 2006) have resulted in rather unsatisfying attempts to solve κ directly using the raw fluxes as they appear in (22), often finding unphysical (large negative values) and noisy distributions with changing signs. Diagnostics have normally shown low correlations between the horizontal fluxes and its parameterization in (22), and several authors have pointed out a general lack of agreement between diagnosed eddy fluxes and the downgradient assumption (e.g., Roberts and Marshall, 2000; Griesel et al., (2009)). This flux-gradient relationship is influenced by rotational components that have been ascribed the main reason for absent correlations and negative, unphysical diffusivities (Bryan et al., (1999). Only the divergent parts of the fluxes, i.e., the components that act on the prognostic budget (1) should be used to estimate the

diffusivity κ. The rotational parts transport equal amounts of tracer into and out of any region, and hence divergence-free. Despite their irrelevance to (1), the presence of these fluxes corrupts and biases the $\overline{\boldsymbol{u}'\rho'}$ term in respect of solving (22) (Eden et al., 2007b).

Rotational and divergent fluxes may in principle be separated using a Helmholtz decomposition (e.g., Jayne and Marotzke 2002). But such a process depends on known boundary conditions to produce unique results (Fox-Kemper et al., 2003), and requires calculations of integrals that are fairly expensive numerically. Marshall and Shutts (1981) instead propose an *approximate* diagnosis of the rotational fluxes through the eddy variance equation in the quasi-geostrophic approximation in which they describe the rotational component fluxes as advection of density variance in the horizontal, i.e., circulating along isolines of constant variance. Having computed the rotational fluxes, these can be subtracted from the total eddy fluxes to find the residual. The MG method is a generalization of the method proposed by Marshall and Shutts (1981), as discussed next in Section 2.4.1.

In order to acquire estimates of the eddy diffusivities that are not compromised by the presence of rotational fluxes, we must assess the residual divergent fluxes relevant for prognostics of water masses. For this we attempt two different approaches. First, an effort is made to subtract most of the rotational components directly from the eddy flux field using a method (2.4.1) suggested by Medvedev and Greatbatch (2004). Secondly, we analyze the *divergence* of the eddy fluxes and the parameterizations (2.4.2). The divergence of vector fields have, by construction, vanishing rotational components, enabling us to compare relevant correlations. Both procedures are elaborated next Results are presented in Section 4.

2.4.1 a) Eddy decomposition per Medvedev & Greatbatch (2004, 2006)

The aim with this approach, hereafter called MG, is a generalization/refinement of the theory by Marshall and Shutts (1981) with a purpose to define a rotational flux, that is associated with the advective component of eddy the variance flux $\overline{\boldsymbol{u}\phi}$ (the variance flux along isolines of mean tracer), while the residual diffusive part is associated with dissipation of eddy variance (diffusive flux across isolines). No assumptions are made

about the mean flow, in contrast to MS assuming that mean flows follow contours of potential density (geostrophic) and purely adiabatic flows. But again, this does not necessarily isolate a residual flux that is *completely* divergence free, so it must be considered an approximation.

The practical result and method presented in the papers of Medvedev and Greatbatch (2004), and demonstrated in Eden et al. (2006) can be written as,

$$\kappa = -\frac{(\overline{\boldsymbol{u}'\rho'} - \boldsymbol{k}\times\nabla_H\theta)\cdot\nabla_H\bar{\rho}}{|\nabla_H\rho|^2}$$

$$\nu = -\frac{(\overline{\boldsymbol{u}'\rho'} - \boldsymbol{k}\times\nabla_H\theta)\cdot(\boldsymbol{k}\times\nabla_H\bar{\rho})}{|\nabla_H\rho|^2} \qquad (37)$$

$$\theta = |\nabla_H\bar{\rho}|^{-2}\overline{\boldsymbol{u}\phi}\cdot(\boldsymbol{k}\times\nabla_H\bar{\rho}) \quad , \quad \phi = \frac{\overline{\rho'^2}}{2}$$

Where θ can be interpreted as a rotational flux streamfunction, the rotational flux component appearing when taking the gradient (rotated 90°). On that account, the only difference from the diagnostic equation (36) presented earlier is a simple subtraction of the defined (MG) rotational flux from the eddy flux, presumably leaving a divergent, residual flux appropriate for diffusivity diagnoses. Eden et al. (2006) and Eden (2007) reports of having successfully removed most regions of unphysical, negative diffusivities through the use of this procedure.

2.4.2 b) Evaluating rotation-free divergences

We have presented a method of evaluation based on explicitly diagnosing the stirring coefficient κ, which is then directly compared with that of the various closure schemes. This approach, however, is inconveniently compromised by rotational fluxes obscuring the relevant divergent residual fluxes. An alternative method is acquired when ignoring the "true" κ and instead regard the divergences of fluxes and the parameterization directly (which is equally relevant since it is the divergence of the fluxes that influences the governing equations). from eq. (22) the horizontal GM skew flux and the downgradient parameterization,

$$\boldsymbol{F}^{H}_{skew} = -\kappa \nabla_H \bar{\rho} = \overline{u'\rho'}\boldsymbol{i} + \overline{v'\rho'}\boldsymbol{j}$$

Taking divergences on both sides yields,

$$\nabla \cdot (-\kappa \nabla_H \bar{\rho}) = \nabla \cdot \overline{\boldsymbol{u}'\rho'} \tag{38}$$

Where κ is the closure to be tested. By definition, the rotational fluxes are eliminated because their divergence is zero. This means, a higher correlation between the left and right hand sides in (37) indicates the better closure (within our framework, set parameters and decisions made during implementation). Results are presented in Section 4.

Note that the divergence of $\overline{\boldsymbol{u}'\rho'}$ could supposedly be influenced by cross-gradient components appearing as an extra term, $\nabla \cdot (-\nu \boldsymbol{k} \times \nabla_H \bar{\rho})$, in eq (22), or by substituting the κ with tensor containing diagonal (diffusive) κ and off-diagonal (advective) ν. But in agreement with the original GM-parameterization and the conclusions by Eden (2010), we may neglect this contribution and focus on the diffusive part of the horizontal eddy flux.

Despite avoiding the complications of rotational fluxes by considering the divergence of the eddy fluxes, many earlier studies have found the correlation between the two terms of eq. (38) to be low and results noisy (Nakamura and Chao., 2000; Solovev et al., 2002, Griesel et al., 2009).

Section 3: The model, methods and set-ups.

This Section briefly describes the data used for computations in this study, the source model and some practical considerations on solving equations (36)-(38) on a discrete numerical lattice based on a terrain-following grid.

3.1 Dynamical properties of the source model

3.1.1 About terrain-following models

Free surface sigma (terrain-following) models (also called σ-models) emerged in the early 1980's, from need to model turbulent processes in proximity of surface or topographic boundary layers (Mellor and Yamada, 1982). Their vertical coordinate were expressed as

$$\sigma = \frac{z - \eta}{D} \tag{39}$$

where η represents the surface deviation from the resting position z=0, and D is the total height of the fluid column.

Such a coordinate system provide a smooth representation of the bathymetry, and is a natural choice for simulating flows close to solid boundaries. In contrast, z (geopotential) models were prone to unphysical interactions due to the "step-like" representation of topography. In addition, the terrain-following type of ocean models elegantly avoided the overflow problem in z models that would result in vanishing surface grid cells (Griffies. 2004). On the other hand, the sigma-models were challenged in accurately describing the pressure gradient, here including a second term (see eq. (43)) to correct for the sloping vertical coordinate lines. The *pressure gradient error* normally becomes significant when these vertical coordinate slopes are steep, that is, when topographic slopes are steep and the correction term gets on the order of the along-coordinate gradient term. A highly accurate numerical

representation is required to avert spurious pressure forces.

3.1.2 The ROMS model (Regional Ocean Modeling System)

ROMS is a community built, open source, state-of-the-art ocean model that with highly advanced physical and numerical algorithms that makes ROMS a more comprehensive program than the otherwise similar POM model. The model is constructed mainly on Fortran 90/95-code and uses C-preprocessing for user input.

The numerical dynamics are resolved on an Arakawa C-grid in the horizontal and *stretched* terrain-following staggered vertical coordinates (Shchepetkin and McWilliams, 2005), which allows better resolution on layers of particular interest or turbulent regions that demand better resolution. It contains algorithms designed to minimize the pressure gradient error. For computational efficiency, the model utilizes a number of barotropic timesteps within each baroclinic timestep. More information is found at www.myroms.org.

There has been little use of this branch of ocean models in publications concerning climate simulations. These models could compliment other types and will hopefully contribute more in future climate research. Sperrevik (2008) demonstrated that ROMS is indeed capable of reproducing experiments performed on a geopotential frame (e.g Marotzke 1997 and Nycander et al. 2007), and produced a climate prognosis for the MOC reasonable and interesting results. It should be noted that studies published on the topic of mesoscale eddy diffusivites are almost (if not entirely) exclusively based on data from z-coordinate models. In that regard it may be enriching to the field to use this kind of data in the current study.

3.2 Our simulation run, 'Nordic 4 km'

Our model domain is 4000 by 2000 km covering the Greenland, Norwegian and North seas, a small portion of the Arctic Ocean and borders the northern part of the North

Atlantic. The rectangular domain is rotated roughly 45° counter-clockwise off the standard north-west directions. The 'x and y' directions are here referred to as xi and eta respectively.

The resolution of about 4km (varying slightly with latitude), should be able to enclose the Rossby radius of deformation in parts of the domain, especially in the southernmost regions and deep-water basins where (baroclinic) wavespeeds are large. The size of mesoscale eddies are usually larger than the Rossby radius (Smith et al., 2000), but scales coherently (locally, as discussed in section 2.3). On our 4 km Arakawa C-grid, we will reasonably permit eddies down to 16 km diameter, but can only expect proper information about eddies of about 40 km and up. This however covers a substantial and conceivably adequate portion of the mesoscale. It is important to note however that even if the model fails to resolve or just partially permit the smaller members of the mesoscale family, the model is *self consistent*; this means that the flow realized in the model are physically complete within its own system. Even if there are smaller eddies in the real ocean, they do not exist in the simulation, so the model's scale cut-off should pose no problem for physical interpretations or be the reason for noisy and incomplete results, as could be the case when working with real-world drifters, etc.

No explicit horizontal viscosity/diffusion (other than the numerical diffusion from the advection scheme to keep solutions stable) were used. Low viscosity retains the fine grained characteristics of the small scale flow we seek to define and parameterize.

3.2.1 Visual demonstration of the resolved dynamics

To gain a firm intuitive sense and cognition of the dynamical processes we study, output values of surface temperature over the last integration year were compiled to an animation viewable at http://www.youtube.com/watch?v=LvgKj5GRrNI.[10] This demonstrates the rich dynamics of the ROMS model and indicates roughly the size of the resolved eddies.

[10] Choose 720 P for the best quality.

3.2.2 Overview of the model domain, bathymetry and the averaged main currents.

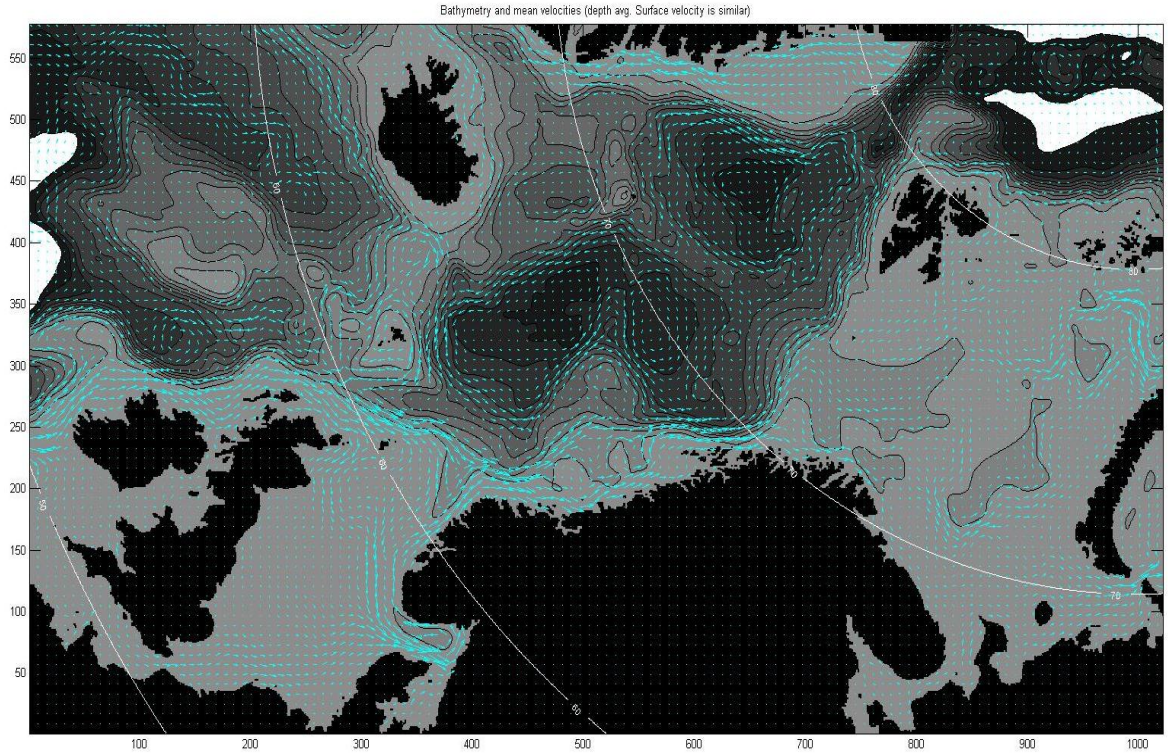

Figure 3.1; The entire Nordic 4 km model domain; colored arrows depict the time-and-depth averaged mean flow, and filled contours illustrate the bathymetry (increasing depth with darker colors). Also shown are latitude isolines.

3.3 Routines and methods used.

3.3.1 On averaging times and spatial smoothing routines.

The density ρ present in our equations were assumed to be potential density, which is more relevant to the adiabatic nature of the fluxes we are studying. It is also a less noisy quantity than the *in situ* pressure. Consequently, we used a uniform pressure identical to surface pressure in our equation of state, $\rho = \rho(T, S, P)$, given by the non-linear relation by Jackett and McDougall (1995).

The eddy density fluxes $\overline{\boldsymbol{u}'\rho'}$ from the model were estimated from equation (4),

$$\overline{\boldsymbol{u}'\rho'} = \overline{\boldsymbol{u}\rho} - \overline{\boldsymbol{u}}\bar{\rho} \tag{40}$$

where the overbar represents a temporal average. The density variance were found by the *sum of squares* method, that is,

$$\overline{\rho'^2} = \overline{\rho^2} - \bar{\rho}^2 \tag{41}$$

Where $\rho' = \rho - \bar{\rho}$, a deviation from the temporal mean ascribed as eddy activity. This is a convenient procedure that requires only one run through the data. We note in passing that one should be vary that calculating a small number as a difference of two large numbers[11] may produce wrong numbers if the larger numbers sustain a minor numerical truncation. This was however tested against a control double-run where the mean were obtained before calculating the deviations directly). Much larger numbers than ~1000^2 must be the case for even 32-bit floats to get truncated.

In eq. (40), $\overline{\boldsymbol{u}'\rho'}$ is meant to account for eddy effects on the density, but changes drastically with the mean densities (and flows) varying by seasonal changes. Therefore these averages must be taken in a series of intra-seasonal, inter-annual means to remove the effects of the seasonal cycle. Eden (2007) used 3-month means, so we initially tried the same. However, less noisy and more convincing results were produced when going even to shorter averaging. This relevant time scale of mesoscale eddy activity has been found to be sub-monthly. Also, three-month averages inevitably picks up signals of seasonal variations in the mean density field. Even monthly averages can be argued to be influenced by seasonal change. Several definitions of eddy fluxes were tested, including deviations from 21, 7 and even 3 day averages. The shortest averaging windows resulted in lower (too low) values of diagnosed diffusivity, indicating that the time scale of the processes we investigate is generally somewhere in between a week and a month.

Despite these precautions, computing even the raw diffusivities from (22) pose new

[11] Which is the case with water density and in turn the basis for the Boussinesq approximation.

questions. It is clear that the variables should be smoothed or averaged spatially over many eddy length scales; we cannot expect the parameterizations to hold everywhere, but taking out the noise should reveal the dominating trend. In analogy to a temperature field, molecules all have different kinetic energies and directions, but the kinetic energy mean field, which is the temperature field, always takes on an exact down-gradient evolution.

Furthermore, taking gradients may quickly increase whatever numerical noise present in our data, rendering some kind of smoothing a necessity. But exactly when and how much to smooth had to be considered and carefully tested. Little information on this were supplied in Eden et al and Eden (2006, 2007), despite the lurking noisiness of the rotational potential θ.

It was necessary to smooth variables prior to taking each gradient. We took precautions to keep the smoothing at a moderate level, preferably at no more grid-points than the typical mesoscale eddies we are studying, which we assumed to be about 40 km in diameter. Hence, some variables were smoothed[12] (spatially averaged) over 10 by 10 grid-points. Smoothing data is not a rigorous practice, but one should respect the specific physical processes and be wary of how such averaging is executed to keep solutions physically sound. In this case, smoothing over the typical scale of a mesoscale eddy should be reasonable.

Marshall and Shutts (1981) assumed that density variance is not transported by velocity perturbations, so that $\overline{\boldsymbol{u}\phi} = \bar{\boldsymbol{u}}\bar{\phi}$. We used the entire variance flux acquired as

$$\overline{\mathbf{u}\phi} = \frac{\overline{\mathbf{u}\rho^2}}{2} - \bar{\rho}\,\overline{\mathbf{u}\rho} + \frac{\bar{\mathbf{u}}\,\bar{\rho}^2}{2} \qquad (42)$$

Where ϕ is half the density variance (eq. (37)).

The θ-term in eq. (37) is described as positive in Eden et al. (2006) but negative in Eden (2007). Both possibilities were tested, and unphysical distributions of diffusivities for negative θ indicated that the term is necessarily positive.

Since our output data stems from a terrain-following, s-coordinate model, a correction

[12] Spatially smoothing data can be seen as averages over a range of eddy length scales.

term is needed for the horizontal gradients in e.g. eq. (28).

$$\boldsymbol{\nabla}_{\mathrm{H}}\rho = \boldsymbol{\nabla}_{\mathrm{S}}\rho - \partial_{\mathrm{z}}\rho\,\boldsymbol{\nabla}_{\mathrm{H}}\mathrm{z} \tag{43}$$

where z is the depth, $\boldsymbol{\nabla}_H$ is a gradient in the horizontal plane a $\boldsymbol{\nabla}_S$ along a constant S-level. These gradients coincide at the surface level and in regions of flat bathymetry.

Section 4: Experiments and Results

4.1 The diagnostics of eddy fluxes and diffusivities

To test the integrity of the horizontal GM skew flux down-gradient parameterization from eq. (22), $\boldsymbol{F}^{H}_{skew} = -\kappa \boldsymbol{\nabla}_H \bar{\rho} = \overline{u'\rho'}\boldsymbol{i} + \overline{v'\rho'}\boldsymbol{j}$, we show the surface eddy fluxes and surface density contours in the Greenland and Norwegian Seas in Figure 4.1. A clear coherence between the fluxes and its parameterization is evident by the downgradient trend of the fluxes. Upon closer examination, however, it becomes apparent that it does not hold for the entire domain; horizontal isopycnal fluxes dominate the diapycnal fluxes[13] in a few regions (for example south of Iceland) i.e., where the parameter ν would dominate κ. This does not necessarily mean that the downgradient assumption is flawed, since it is only concerned with the divergent component that affect the tracer budgets. Rotational components could be present in this picture, and removing them would result in different diagnosed fluxes.

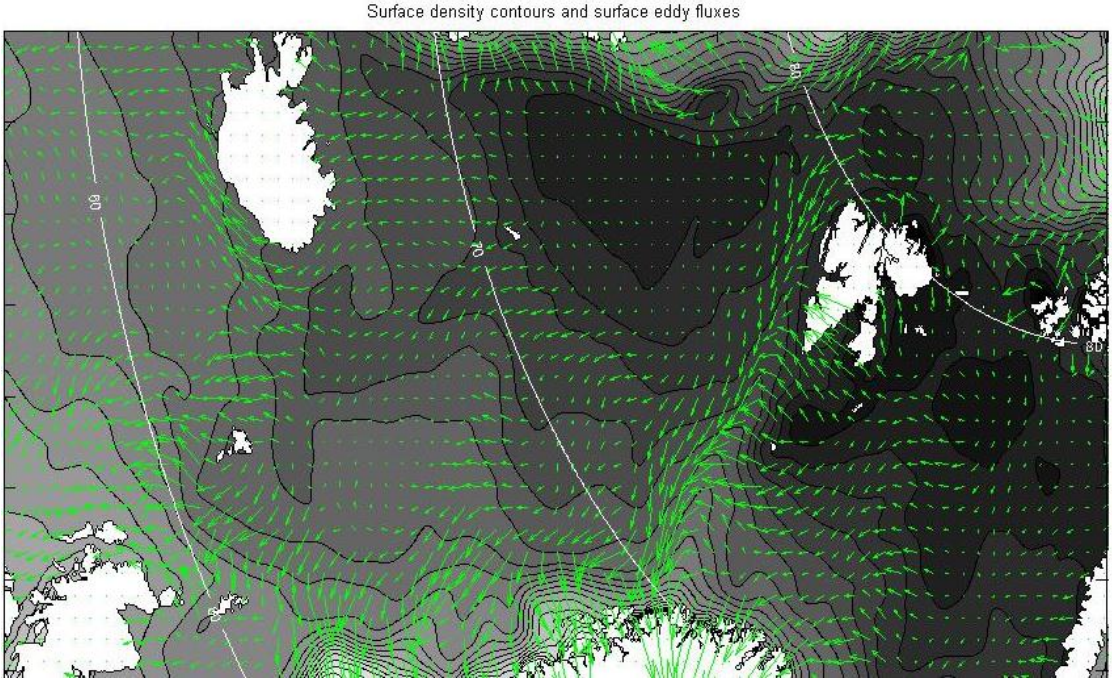

Figure 4.1; Temporal averaged surface density eddy fluxes $\overline{\mathbf{u}'\rho'}$ *are illustrated by green arrows and the surface density field represented by filled contours, where darker colors*

[13] Note that diapycnal fluxes also have a vertical component. Fluxes that are horizontally diapycnal may be isopycnal (adiabatic) in all three dimensions, which is fundamental to the GM parameterization. The skew flux takes on a diffusive role only in the horizontal plane.

represent denser water. Data are smoothed over a window of 15 by 15 grid-points.

The rotational, non-divergent part of the fluxes as assumed by the MG-theory to be $\boldsymbol{k} \times \nabla_H \theta$, is shown in Figure 4.2. A conspicuous, and perhaps suspicious, observation is that the magnitude of the rotational fluxes turned out to be as large and some places larger than the original fluxes. This despite the fact that the θ-field was smoothed extensively (as much as taken to be physically reasonable) before taking the gradients, consequently reducing the gradients of the noisy quantity θ. Griesel et al., (2009) argue that the rotational component is vastly dominating the divergent component based on the observation that the curl of eddy fluxes is generally much larger than the divergence. Although we raise question to their reasoning[14], the results of the MG equation indicate that their statement may be true in this case. Considering geostrophic and rotating motion one could also intuitively expect this. If so, it is clear that we seek, from eq. (37), a small divergent part that is given by the difference of two much larger numbers; a warning sign that obliges for extra precaution.

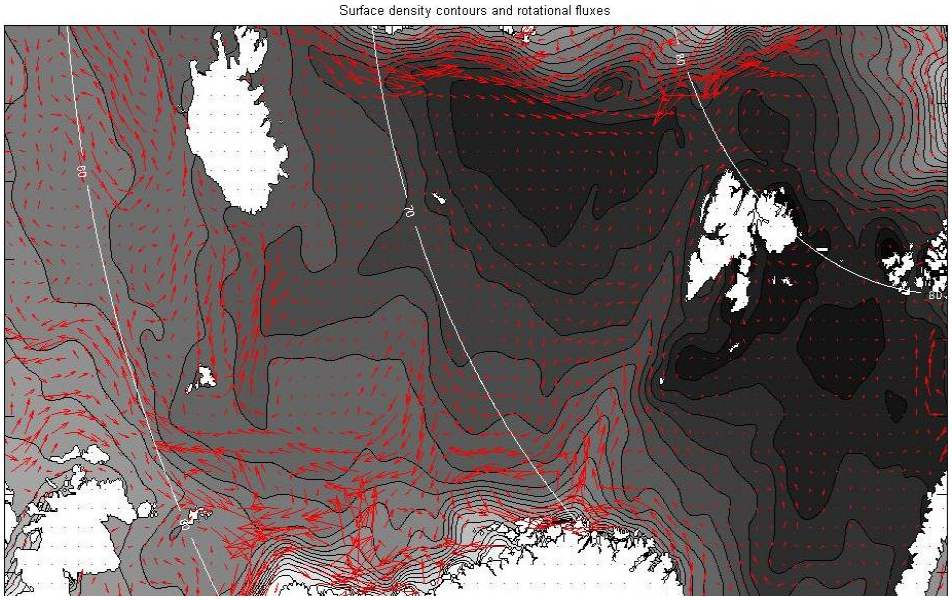

Figure 4.2; Temporal averaged surface rotational density fluxes $\mathbf{k} \times \nabla_{\mathrm{H}} \theta$ *are illustrated by red arrows and the surface density field represented by filled contours. Data are smoothed over a window of 15 by 15 grid-points. Darker colors represent denser water.*

[14] We advocate that the divergence and curl of a vector field may not be used as unique measures for the divergent and rotational component. Even if $(\nabla \times \boldsymbol{F}) \gg (\nabla \cdot \boldsymbol{F})$, the rotational component does not necessarily dominate the divergent.

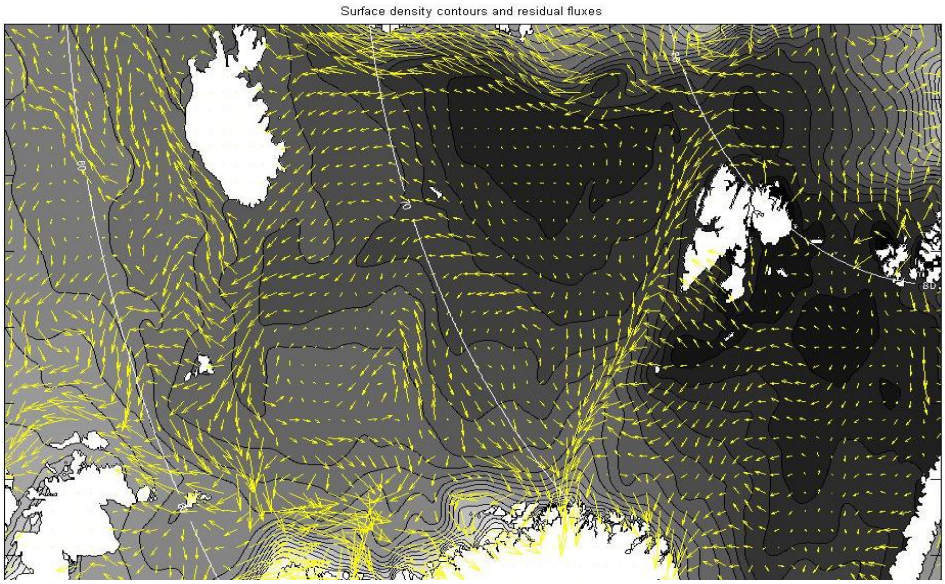

Figure 4.3; Temporal averaged surface density eddy fluxes $\overline{\mathbf{u}'\rho'}$*, minus rotational density fluxes* $\mathbf{k} \times \nabla_H \theta$*, are illustrated by yellow arrows. The surface density field represented by filled contour. Darker colors represent denser water. Data are smoothed over a window of 15 by 15 grid-points.*

A small error or uncertainty in the estimation of the larger rotational flux will greatly affect the relative size of the residual divergent flux. Thus a successful extraction of the divergent component would require high quality data and precise implementation methods. Since the MG method is an approximation, extracting meaningful divergent components may pose a formidable challenge.

Figure 4.3 indicates that the residual fluxes have, in fact, a lesser downgradient alignment than the total eddy fluxes as seen in Figure 4.1.

4.1.1 A direct (raw) diagnostic of κ.

Eq (28) decomposes to,

$$\kappa_{raw} = \frac{\overline{u'\rho'} \cdot \partial_x \bar{\rho} + \overline{v'\rho'} \cdot \partial_y \bar{\rho}}{|\partial_x \bar{\rho}|^2 + |\partial_y \bar{\rho}|^2} \qquad (44)$$

Solving this equation at each point in our three-dimensional space should give us a direct diagnosis of the magnitude and distribution of the *raw* diffusivities. In this context, *raw* means the total fluxes with both the divergent and the inconvenient

rotational fluxes present. The estimation of κ is illustrated in Figure 4.4. Despite the apparent noise, it gives a decent indication on how κ is distributed throughout the Nordic seas, in respectively depth averaged values (upper left), surface values (upper right, notice the scale change) and, a vertical section of horizontally averaged data (bottom pane). The highest values of κ are found in a belt loosely related to the North Atlantic Current (NAC), with a diffusive hot-spot in the NAC region south of the Faeroe Islands that continues along the Iceland-Faeroe ridge. Considerable diffusivities appear in the transitional region Barents- and Norwegian Sea. In the quiescent, abyssal regions of Greenland sea, and the gyres of the Norwegian sea, there are, as expected, little depth averaged eddy activity and low values of κ. The North Sea imparts chaotic regions with diffusivities of alternating sign. The Barents sea also show traces of negative diffusivities.

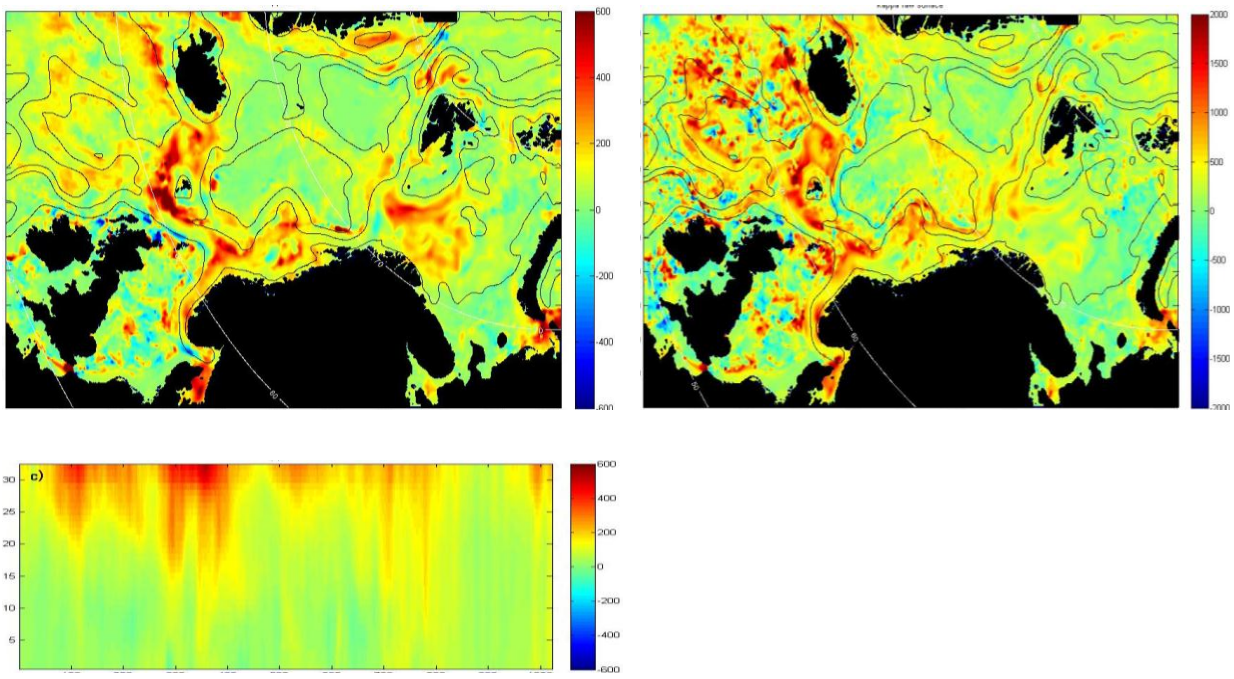

Figure 4.4; Distributions of diffusivities κ. The upper left pane depicts depth-averaged values, the upper right surface values (note the scale change). The lower pane represent a vertical section of horizontal average ignoring landmasks. Note that the vertical figure displays s-coordinates rather than physical height, but show clear trends of depth decaying diffusivities.

It is evident that diffusivities diminish with depth, consistent with observations of eddy energy levels (Gent, 2010). The shown horizontally averaged values of κ (bottom pane) ranges from slightly negative to almost about 800 m^2/s by the upper

layers, but do not appear to concede to the overall canonical mean magnitude of 800 m^2/s (Danabasoglu, 2004). If a spatially constant value were to be suggested based on this particular diagnosis, it would be closer to 300 m^2/s.

One should note of the lack of negative regions that were expected on account of diagnoses made in other studies; large regions of unphysical, negative diffusivities have dominated many previous results and have remained a bothersome artifact (as discussed in Section 2.4). Our diagnosis show some telltale signs of negative contributions, but only in limited areas, fully receding when taking a horizontal mean. Persistent negative diffusivities have commonly been explained as a consequence from the complications by rotational fluxes (e.g., Bryan et al., 1981; Eden et al., 2006). The cause of the contrast to our result is not clear. It was evident from Figure 4.1 that most of the raw eddy fluxes comprised a dominant down-gradient (horizontally diapycnal) projection, affording positive κ. But even if our current data look and seem plausible, presence of rotational fluxes may have, and probably have, warped the estimation to some degree.

4.1.2 Subtracting the MG rotational components.

Eq. (29) takes on the following form when decomposed,

$$\kappa_{\mathrm{MG}} = -\frac{\left(\overline{u'\rho'} + \partial_y\theta\right)\cdot\partial_x\bar{\rho} + \left(\overline{v'\rho'} - \partial_x\theta\right)\cdot\partial_y\bar{\rho}}{|\partial_x\bar{\rho}|^2 + \left|\partial_y\bar{\rho}\right|^2}$$

$$\theta = \frac{\overline{u\phi}\cdot\left(-\partial_y\bar{\rho}\right) + \overline{v\phi}\cdot\left(\partial_x\bar{\rho}\right)}{|\partial_x\bar{\rho}|^2 + \left|\partial_y\bar{\rho}\right|^2} \tag{45}$$

where the $\overline{\boldsymbol{u\phi}}$ vector are given by eq. (37), describing advection of density variance, $\phi = \frac{\overline{\rho'^2}}{2}$.

Eq. (45) is similar to (44), but where rotational fluxes, as assumed by Medvedev & Greatbatch (2004), have been subtracted from the raw fluxes. Figure 4.5 presents the distribution of κ_{MG} as given by eq. (45). It is immediately noticeable that this result contain more noise compared to κ_{raw}. The magnitude has also generally increased.

The most significant diffusivity intensifications appear at the Iceland-Faeroe ridge, the Barents-sea and along certain parts of the NAC including near the west coasts of Britain and Norway.

An evident anomalous outcome of the MG method is the intense negative diffusivities appearing in assorted regions, mostly over ridges and steep slopes in the bathymetry. This behavior was persistent through various methods of temporal averaging and spatial smoothing.

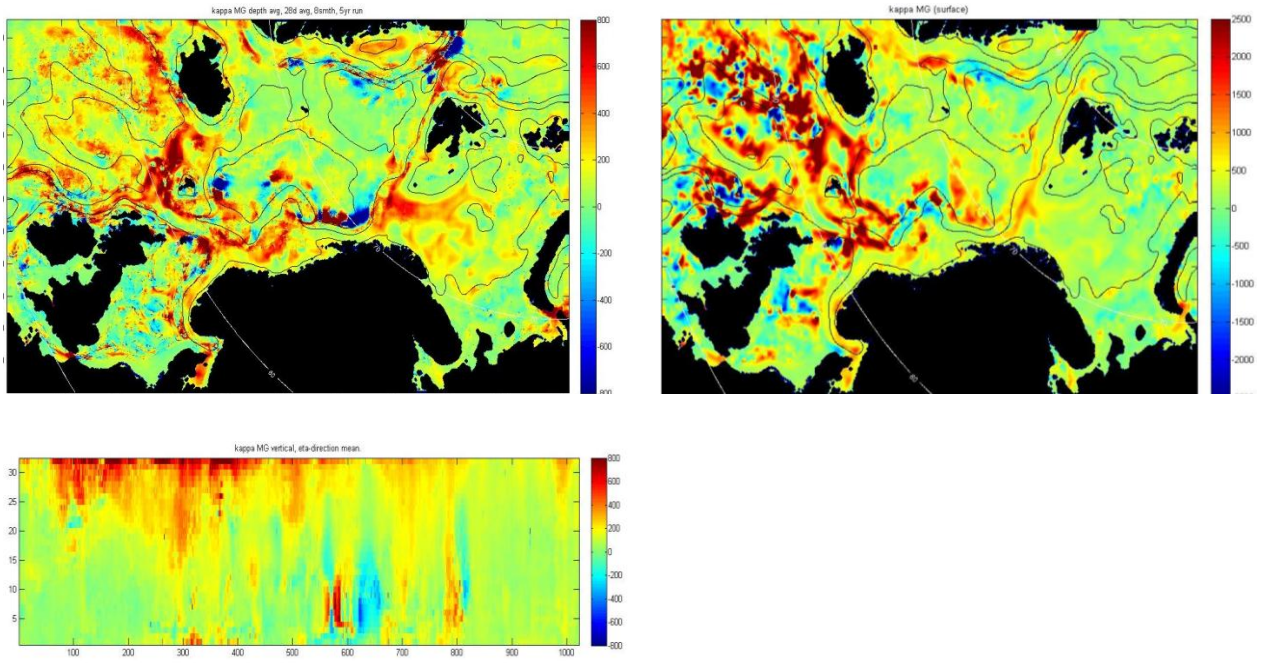

Figure 4.5; Surface distribution of MG-diffusivities as given by eq. (45). Diffusivities range from 0 to over 2000 m^2/s, with negative values appearing only a very few places. More pronounced diffusivities (compared to Figure 4.4.), both negative and positive, appear throughout the domain.

The rise of negative regions was highly surprising, since getting rid of negative diagnostics of κ has been a key motivation for attempts to separate divergent and rotational eddy fluxes. In this interest, we observed the opposite effect. Of course, κ_{raw} presented rather few negative regions that could possibly be sign-corrected. It could be that the MG method primarily works over larger (negative) areas and may induce local increase of negative diffusivities.

Also, physical explanations may exist for negative diffusivities in limited regions, and one should not be tempted to promptly dismiss the validity of κ_{MG}. The appearance

of intense negative regions happens almost exclusively near steep topography (in the depth average case), which is regions where solid boundaries may influence the effect of eddy processes. Furthermore, the increase of mixing strength arriving with the MG method is a step closer to accordance with mean coefficients earlier estimated as high as ~ 800 m^2/s (Danabasoglu, 2004). This number is far from conclusive, however. Many of studies have attempted to diagnose κ, but only a gross overall magnitude suitable for large scale applications can be firmly concluded, varying from regions of 0 to over 5000 m^2/s, and in some cases extreme local values over 10.000 m^2/s have been reported (e.g., Rix and Willebrand, 1996; Nakamura and Chao, 2000; Roberts and Marshall, 2000; Solovev et al., 2002, Eden et al., 2006; Tanaka et al., 2007; Griesel et al., 2009) Most studies have been carried out on different models and types of computational domains, making a good first guess for what kind of values we could expect in our limited region case difficult. For instance, simulations in Eden et al. (2006) and Eden (2007) show occasional large regions (up to the very size of our domain) of almost vanishing diffusivities while other equally large areas exhibit over 3000 m^2/s. No previously published studies known to us have estimated diffusivities in the Nordic Seas, so no direct comparison is available. The results of κ presented so far appear as physically reasonable in both magnitude and distribution, however. To that resolve, we have obtained a foundation to which the output from the various diffusivity closures may be compared.

4.2 Trial A: Comparison of closures and diagnoses

Four different closures, EG, VMHS, NSQR and VMHS/NSQR were diagnosed based on monthly averaged variables and summed up (similar to the procedure with the direct diagnoses). As established in Section 2.3.4, the latter is a combination closure motivated by the strictly horizontally dependent VMHS, and depth-only dependent NSQR. None of these results are exact replica of those presented in Eden et al. (2008), but slightly adjusted to produce the most compliant (with each other, the direct evaluation and intuitive knowledge) results. For instance, due to the high latitudes we work in, the Rhines scale- dependence were dropped from the EG closure and rather

introduced a modest dependency on the local grid scale. The tuning parameters of VMHS and NSQR was respectively increased and reduced in comparison to earlier suggested tuning (ED08). The essential physical characteristics of the closures were however maintained. Variables are smoothed over 5 by 5 grid points, prior to computation of κ.

Figure 4.6 illustrates how diffusivities, as produced by these closures, are distributed in our domain (for comparability, the lower part of the color scale is reserved for negative diffusivities that appear in direct estimates). Despite being fiercely distinct in some regions, they do pick up many of the same characteristics. All schemes produce high diffusivities in the northern Atlantic west of Great Britain, continuing in a belt roughly following the NAC along the coastal regions of Norway and along the West Spitsbergen current. All closures show minima in the quiescent, abyssal gyres of the Norwegian and Greenland seas, as well as the Arctic Ocean north of Spitsbergen, all on general accord with the distribution of the direct diagnose of κ.

All schemes concur on a hotspot of diffusivities along the Faeroe-Iceland ridge. In the Barents- and North Seas, VMHS and EG pick up only a modest signal of diffusivities, while NSQR in contrast produces intense diffusivities in these regions in disagreement with the direct diagnosis.

It is clear that all closures are heavily influenced by the underlying topography (illustrated by black lines). In this regard one should also notice the veins of high diffusivity found along the topographic ridges like the Vøring-plateau in VMHS and to some degree EG (but not in NSQR). In such regions the topography normally places a strong constraint on the flow (topographic steering is obvious in Figure 3.1), often suppressing eddy activity in such regions. The mean-flow dependent closures, on the other hand, find strong local gradients and predict increased diffusivity where there should probably be less. This unphysical defect also occur inside strong currents. Ferrari & Nikarushin (2010) suggest a technique to reduce this kind of local overrepresented diffusivities (Section 4.2.1). The surface values of the same experiments are shown in Figure 4.7, demonstrating a much lower coherence among the closures than for the depth averaged analogue (Figure 4.7).

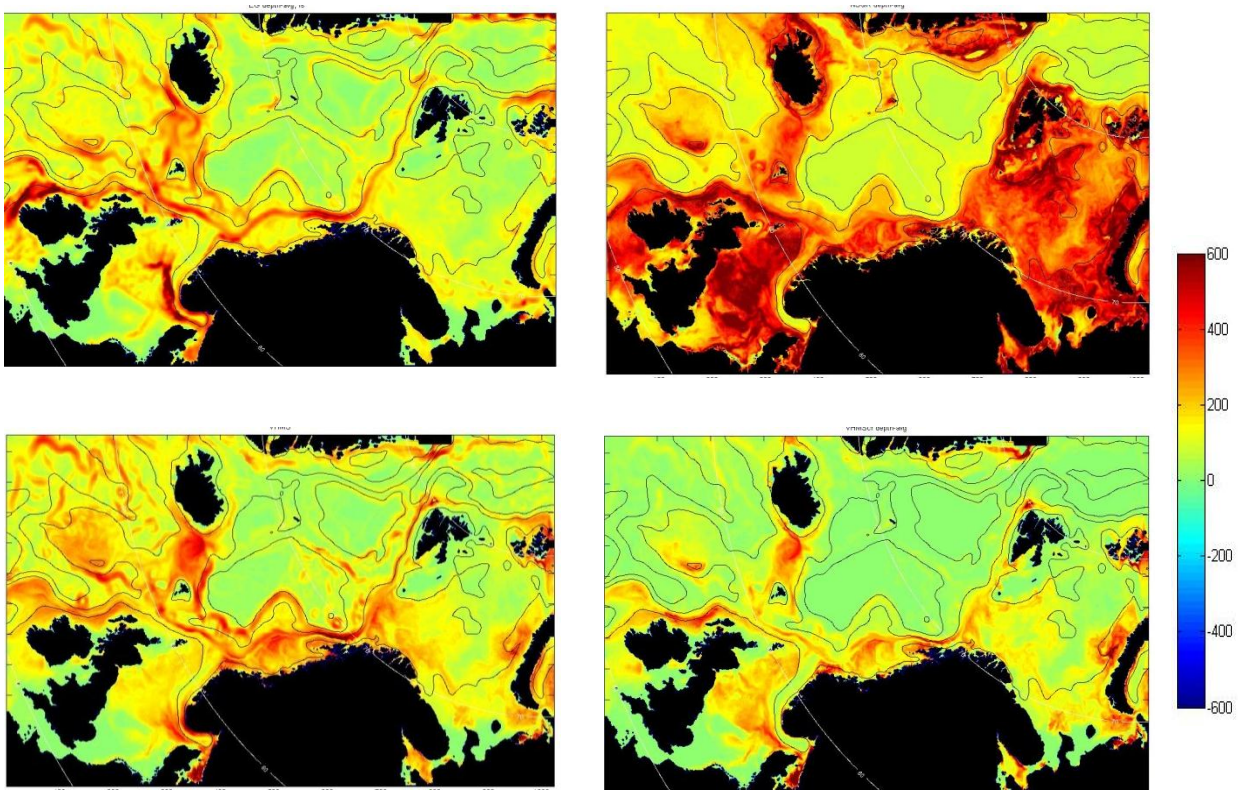

Figure 4.6a; Depth averaged values of κ for closure EG (top left), NSQR (top right), VMHS (bottom left) and VMHS/NSQR (bottom right). Also shown is bathymetry contours (black lines) and lines of constant latitude (white lines). The actual values may be tuned using a parameter, so the main interest of the figure is the actual distribution.

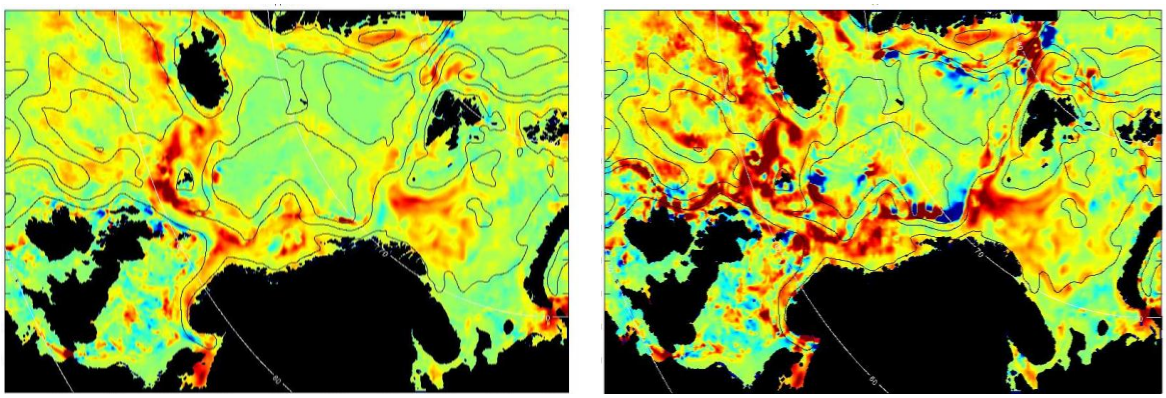

Figure 4.6b; Depth averaged values of κ_{raw} and κ_{MG}, copied from Figure 4.4 and 4.5 for easy comparison to Figure 4.6a, and use the same color scale.

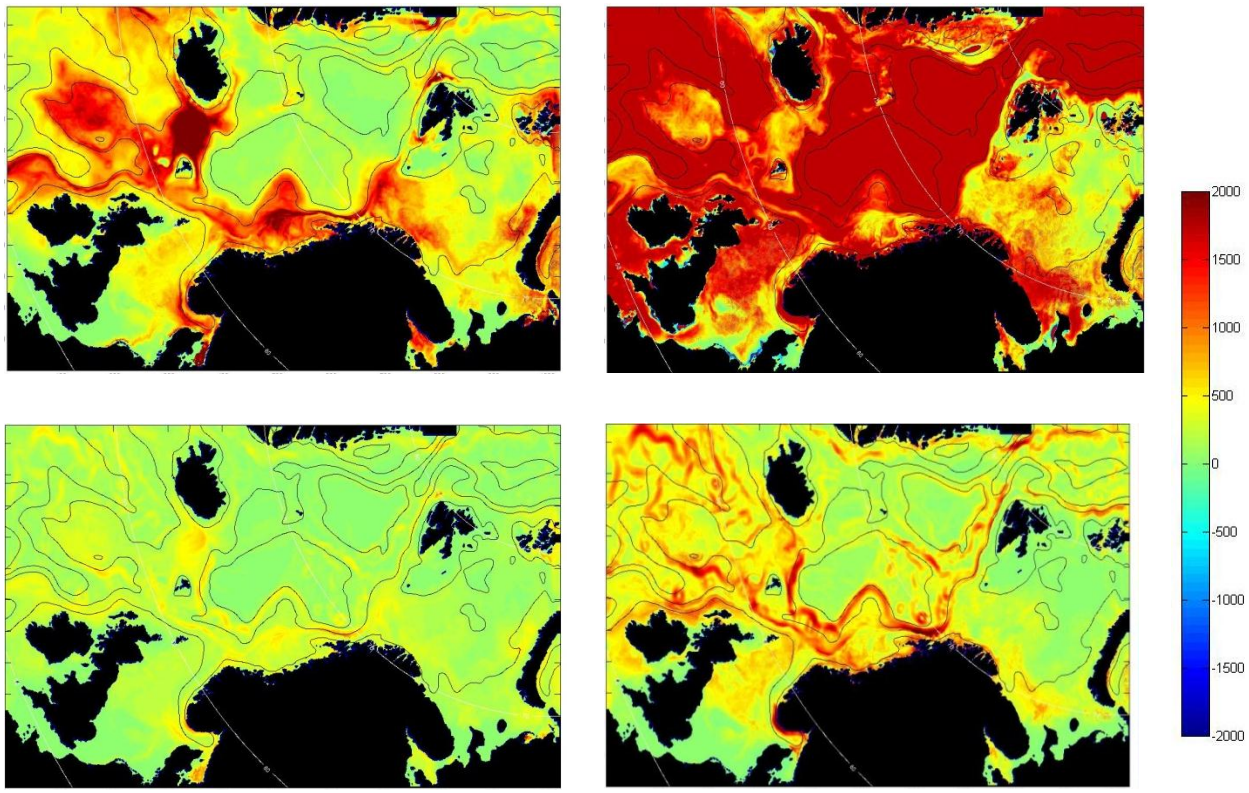

Figure 4.7a; Surface values of κ for closure EG (top left), NSQR (top right), VMHS (bottom left) and VMHS/NSQR (bottom right). Also shown is bathymetry contours (black lines) and lines of constant latitude.

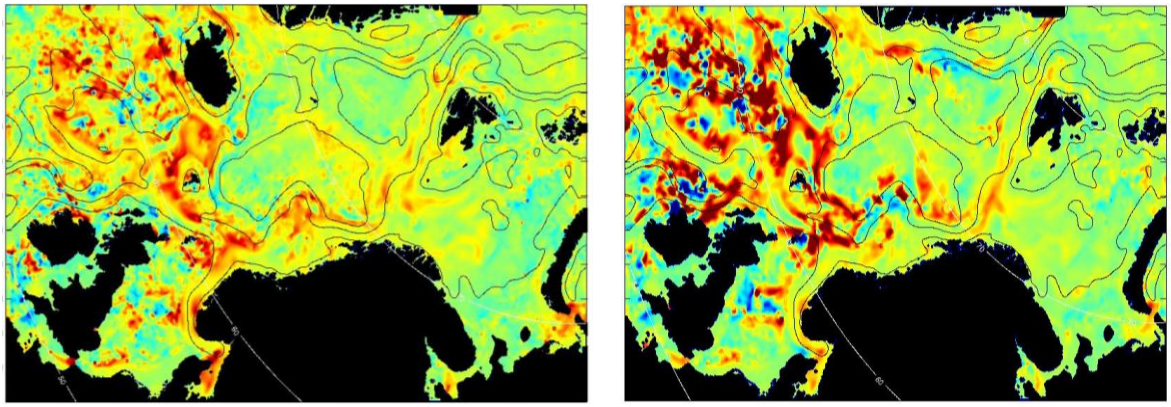

Figure 4.7b; surface values of κ_{raw} (left) and κ_{MG} (right) copied from Figure 4.4 and 4.5 for easy comparison to Figure 4.7a.

The first thing to notice is NSQR's unphysically high mixing in the surface of the deep basins of the Norwegian and Greenland sea, where low diffusivities are expected. This is a consequence of the pycnocline reaching the surface in these parts

of our model domain (no presented mixed layer). It follows that the buoyancy frequency N in (31) finds its maximum (equal to N_{ref}) This extreme surface diffusivity however, decays rapidly with depth and so the depth averaged plot (Figure 4.6) correctly reflects the diminishing values of eddy mixing in these regions.

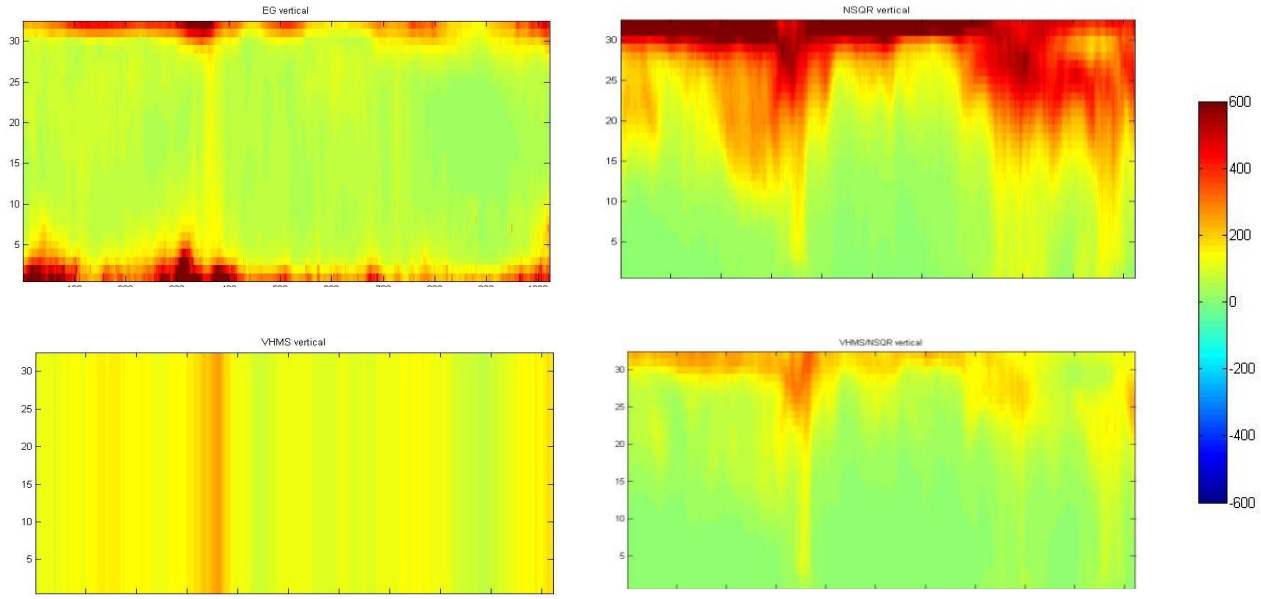

Figure 4.8a; Diffusivities (m^2/s) *averaged over the eta-direction (south-east to north-west) ignoring land-masks, showing the vertical dependence for closure EG (top left), NSQR (top right), VMHS (bottom left) and VMHS/NSQR (bottom right). Caution; these plots show averaged values along constant s-layers only, not height. The essential trends of decaying κ are nevertheless clear.*

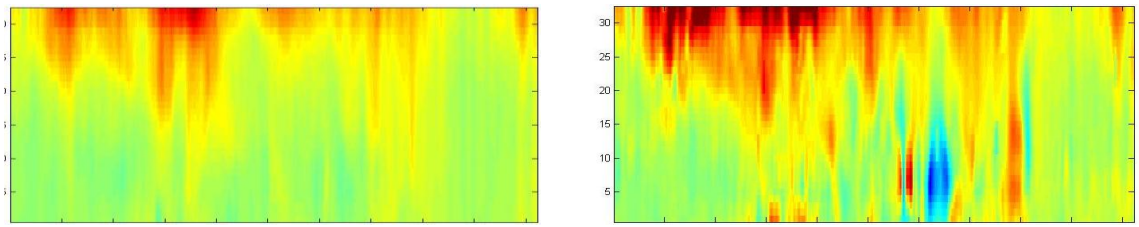

Figure 4.8b; surface values of κ_{raw} *(left) and* κ_{MG} *(right) copied from Figure 4.4 and 4.5 for easy comparison to Figure 4.8a. The color scale is identical.*

VMHS appears to produce very low values at the surface plots. This is simply because of the scale change between Figures 4.7 and 4.8; VMHS is vertically constant and therefore grants lower surface values than the vertically dependent schemes that intensifies eddy mixing with lesser depth (see Figure 4.8)

Figure 4.8 reveals a trend of diffusivities decreasing with depth (except for VMHS). Closure EG also exhibit an increase of mixing in proximity of topography, that must be a spurious effect caused by the vertical velocity shear taking place close to topography (and especially near slopes), an incentive for the closure to predict excessive eddy mixing due to increase of eq. (34). This artifact should be trivial to avoid during implementation in ocean models, and should be ignored in the evaluation process.

4.2.1 Ferrari-Nikarushin Suppression

In Section 2 it was stated that the enhanced diffusion analogy between eddies and molecular diffusion holds as long as there is a sufficient separation of time scales (Papanicolaou and Pironneau, 1981). However, eddy diffusivities can be strongly modulated by variations in the large-scale currents, as eddies propagate at a speed proportional to, but smaller than, that of the mean flow that engulfs them (Vallis, 2005). Consequently, diagnostics may overestimate eddy activity in such regions. This issue with eddy mixing is mostly an ignored topic in the literature, but argued by others to be a crucial feature (e.g., Andrews et al. 1987). Indeed, our experimental diagnostics of EG and VMHS exhibit pronounced veins of intense diffusivities along the main currents that is not indicated by the direct estimation (Figure 4.4).

This problem was acknowledged by Ferrari & Nikurashin (2010), who suggested that diffusivities in main currents should be dampened when the ratio between mean kinetic energy and eddy kinetic is large, as one should expect from inside core jets. In their paper they worked with the diffusivity estimation of Holloway based on the early satellite altimeter data (Keffer and Holloway, 1988), but the essential finding in that paper could easily be (approximately) applied to our diffusivity closure experiments by establishing,

$$\kappa_{fs} = \frac{\kappa}{1 + d \cdot \frac{MKE}{EKE}} \tag{46}$$

Where κ our pre-diagnosed diffusivity in each point, κ_{fs} is the 'suppressed' diffusivity, and d is a tuning parameter suggested to be about 8. MKE and EKE are

mean kinetic energy and eddy kinetic energy respectively. This ratio is presumably largest (MKE will dominate) in core jets. In turbulent regions without pronounced mean flows, EKE will dominate and the diffusivity will remain largely unchanged. Applying this to the results of VMHS (figure 4.6), yields a subtle difference described by Figure 4.9.

a)

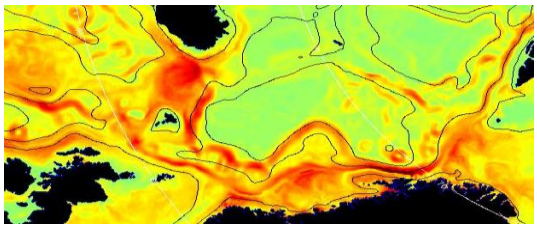

b)

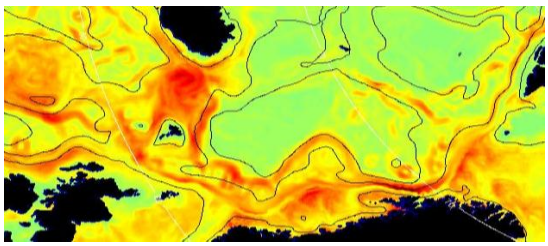

Figure 4.9; a) Close-up of the VMHS depth-averaged output from Figure 4.7. A Ferrari-Nikarushin Suppression is applied to the fields (b), slightly reducing the diagnosed diffusivities along topographic and inside main currents but largely maintaining intensity elsewhere.

The kinetic energies were estimated monthly as $EKE = \frac{1}{2}\overline{\boldsymbol{u'^2}} = \frac{1}{2}(\overline{\boldsymbol{u}^2} - \overline{\boldsymbol{u}}^{\boldsymbol{2}})$ and $MKE = \frac{1}{2}(\overline{\boldsymbol{u}}^{\boldsymbol{2}})$ where $\boldsymbol{u} = (u, v)$ is the horizontal velocity, vertical kinetic energies being neglectible.

The suppression method only slightly reduced the estimated diffusivity at topographic ledges and main currents. Tuning up the parameter *d*, eq. (46) significantly suppressed the entire diffusivity field. This is because EKE and MKE are strongly correlated, resulting in an almost uniform reduction of κ using too high suppression parameter.

High correlations of MKE and EKE is not merely a regional characteristic of our domain, but a common property as well (Eden, 2007)[15] A subtle improvement was however evident, and was used hereafter in our experiments, more specifically in closures VMHS, EG and VMHS/NSQR.

[15] Eden 2007 nevertheless notes an exception in the rapid flowing Malvinas current east of south-America. Attached and stabilized by the pronounced continental slope, it demonstrates high MKE and low EKE.

4.2.2 Diagnostic-Closure Correlations

Four closures were tested; one horizontally dependent only (VMHS), one only (locally) vertically dependent (NSQR), and two dependent on both. A careful comparison of similarities found in Figure 4.6 through 4.8 may suggest which closure that best recognized and recreated the conditions for eddy strength in our domain. Assuming, of course, that our direct diagnoses of diffusivities are amply accurate. The main features were by large satisfactory described, for instance the calm abyssal regions and the stronger mixing along and outside main currents and the moderate levels in the Barents Sea and the northernmost Atlantic. The intense hotspot south of Faeroe Islands were underestimated by all closures, in contrast to the low (but chaotic) diffusivities of the North Sea that were generally overestimated.

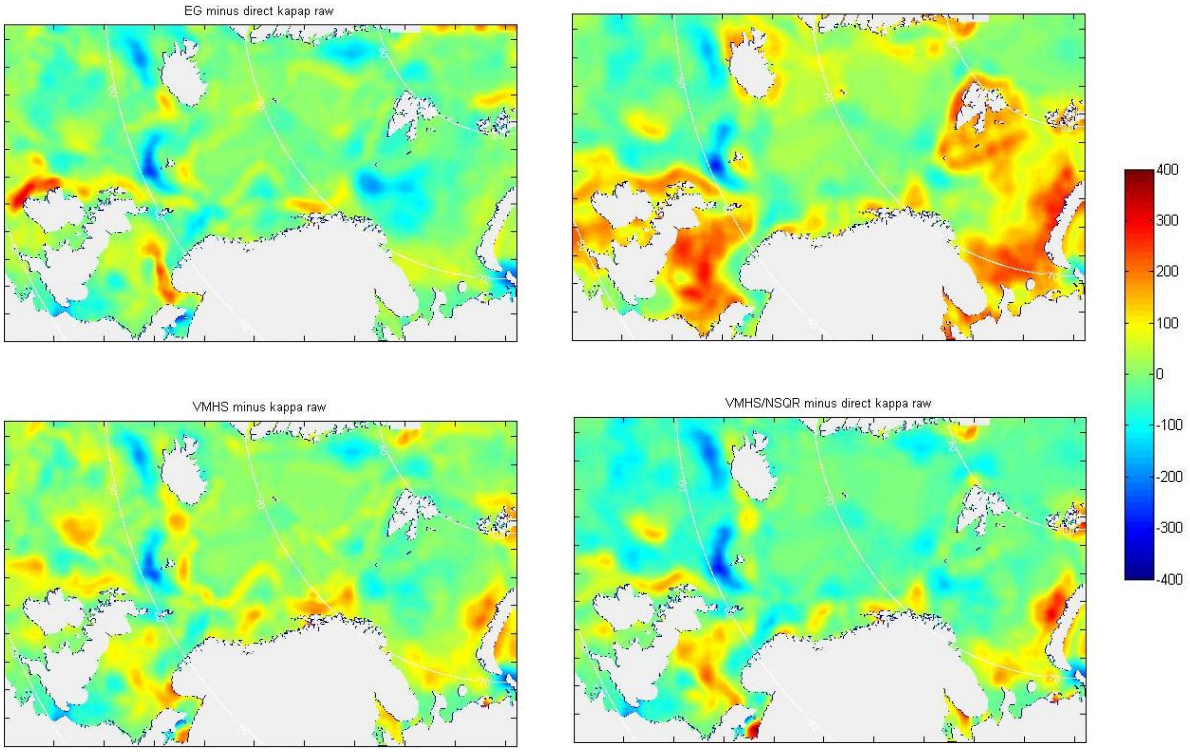

Figure 4.10; Differences (biases) between the directly diagnosed diffusivity and each closure (depth averaged). Data are smoothed over 15 by 15 grid points. From top right to bottom left: a) EG, b) NSQR, c) VMHS, d) VMHS/NSQR.

In VMHS and EG, Ferrari suppression moderated exaggerated diffusivities over

continental slopes. NSQR seemed inadequate to capture the dominant characteristics, and several places gave very high values of κ when the opposite were desired, for instance, in the North Sea, Barents Sea and the entire region around Spitsbergen and stretching south. These trends are visible in Figure 4.11, where the bias, i.e., difference between the closure and the direct calculation (still depth averaged) are illustrated. Overestimations are shown in red and underestimations in blue. All data are smoothed over 15 by 15 grid points for more appropriate comparisons in terms of eliminating noise and to simulate the conditions of a coarse gridded model (recall that point values in such models are equivalent to spatial averages in finer grids, (3)). Additional spatial smoothing would enhance the correlation, but could also cancel out much of the differences between the closures.

The values displayed in Figure 4.10 are only biases, in the sense that they can easily be adjusted higher or lower with a simple parameter. Of course, reducing bias one place increases negative bias elsewhere, and vice versa. In the depth-averaged test, VHMS produces the best fit with a correlation coefficient of 0.71. This is illustrated in Figure 4.11, where each point in (depth averaged) space is mapped as a function of the diagnosed and the (closure) estimated κ. VMHS show the clearest trend resembling a diagonal line. At the same time NSQR shows a poor correlation and an inability to produce wide enough horizontal variability of κ. For instance, the $\kappa_0$value appears, by construction, in every column. To bring NSQR to optimal terms with the direct diagnosis, we found that κ_0 should be substantially reduced from 4000 to under 2000 m^2/s , eq. (31). Our suggested closure (d), the combination of VMHS and NSQR is an improvement over the constant reference value. It suffers from the symptoms of NSQR that unwarranted high estimations appear in regions that should have little eddy activity. Because of this, EG (a) makes less extreme errors, and has a more uniform bias, but may have a slightly wider spread a low values. EG also produced in general too strong diffusivities, and we suggest lowering the tuning parameter c (31) from 2 to 1.5.

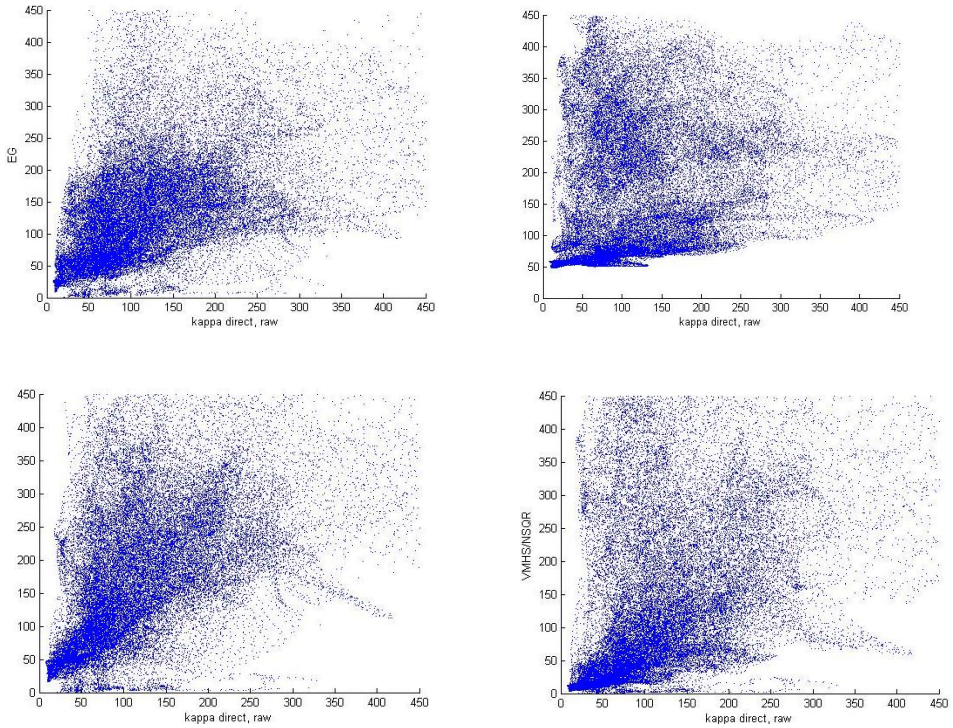

Figure 4.11; Correlations between κ raw and the individual closures for depth averaged values. Each point in space produces a value from both the closure and direct calculation, mapped above. A tighter diagonal line means higher correlation. From top left to bottom right: a) EG (0.63), b) NSQR (0.49), c) VMHS (0.71), d) VMHS/NSQR (0.56). The numbers in parenthesis are the associated correlation coefficients.

In verdict of the depth-averaged case, VMHS (c) seemingly performs best with a correlation coefficient of 0.71, whereas EG comes second with 0.63. The depth modified VHMS seems to be an improvement from using a constant reference value. For horizontally averaged cases, on the other hand, VMHS appears inadequate due to its depth independence. Many modeling communities have acknowledged the importance of vertically varying mixing intensities and have progressed to other closures. In this regard, the EG closure indeed seems a good candidate. But then, comparing Figure 4.8a and Figure 4.8b, it appears that the direct diagnosis show a depth decaying trend that resembles that of NSQR (and VMHS/NSQR) more than EG. Here our suggested combination closure may prove its use.

All correlation coefficients are summarized in table 4.1, including comparisons for surface values and correlation with the κ_{MG}- distribution. Each case are tested with two different amounts of spatial smoothing, 3×3 and 20×20 grid points. It is reasonable to consider scale-averaging over such magnitudes, since coarse resolution models appropriate for this type of parameterizations require averaged, large scale fields. But excessive smoothing may conceal fine scale similarities between divergence fields, motivating a test of both.

	κ_{raw} surface		κ_{raw} depth-avg		κ_{MG} surface		κ_{MG} depth-avg	
	Lo	Hi	Lo	Hi	Lo	Hi	Lo	Hi
EG	**0.45**	0.67	0.36	0.63	0.33	0.57	0.31	0.56
NSQR	0.30	0.40	0.33	0.49	0.29	0.50	0.22	0.34
VMHS	0.44	0.66	0.47	0.69	0.34	0.59	0.36	0.63
VMHS (FS)	0.44	0.67	**0.48**	**0.71**	0.34	0.59	**0.37**	**0.64**
VMHS/NSQR	0,43	0,70	0,34	0,55	0,36	0.62	0,28	0,47
VMHS/NSQR (FS)	0,44	**0,71**	0,35	0,56	**0,37**	**0,63**	0,28	0,46

Table 4.1; Diagnosed eddy diffusivities are compared to diffusivities obtained from the closures and presented in terms of correlation coefficients. In each case, both surface and depth averaged output are compared using low and high effective spatial smoothing on each field.

The forth column in Table 4.1 corresponds to the comparisons made in association with Figure 4.10 and 4.11, that is, depth-averaged fields and high data-smoothing.
The proposed VMHS/NSQR closure obtains the higher correlation in terms of surface comparison to either diagnosed field, but lower quite low for the depth averaged case. In general terms, the closures show a better correlation with the κ_{raw} field. Specific correlations for the vertical profile (horizontal average) are not shown, but the NSQR-based closures are the only ones with significant correlation, as illustrated by Figure 4.8. Note also that the Ferrari-Nikarushin suppression in most cases slightly improve the correlation coefficient.

4.3 Trial B: Comparison by divergences

Reciting eq. 37, taking the variance on each side of the horizontal skew flux equation (22) yields,

$$\boldsymbol{\nabla} \cdot (-\kappa \boldsymbol{\nabla}_{\mathrm{H}} \bar{\rho}) \;=\; \boldsymbol{\nabla} \cdot \; \overline{\mathbf{u}' \rho'} \qquad (47)$$

As discussed in Section 2.4, assessing the divergences of the fluxes and the parameterization will, by definition, eliminate the complications in a diffusivity diagnosis caused by rotational components that may be present in the eddy flux field. In this section we evaluate which input for κ that produces a best fit for the *divergence* of the downgradient parameterization (47) compared to the divergence of the eddy density fluxes. Seven different input values are tested including the four closures, the raw diagnostic, the MG diagnostic and a constant value.

Figure (4.12) displays divergences of the direct eddy fluxes $\boldsymbol{\nabla} \cdot \; \overline{\boldsymbol{u}' \rho'}$ in the upper left pane, and the divergence of the downgradient parameterization $\boldsymbol{\nabla} \cdot (-\kappa \boldsymbol{\nabla}_H \bar{\rho})$ for κ_{const}[16], κ_{raw} and κ_{MG} respectively.

It is immediately apparent that the flux and parameterized fields are highly similar (in contrast to findings in other studies, e.g., Nakamura and Chao, 2000;. Griesel et al., 2009. This provides confidence to the validity of the down-gradient (horizontal skew flux of density) parameterization of mesoscale eddies. More specifically, one should notice the especially striking similarity between the divergence of the eddy fluxes and the downgradient parameterization using the raw diagnostic of kappa (Figure 4.12a; upper left, bottom left). This also raises confidence to the use of our (raw) diagnostic as a good estimate, and in turn an appropriate frame of reference for comparing and evaluating optimal quantifications of eddy diffusivities. If the raw diagnosis were indeed highly corrupted by rotational components, the correlation between the divergence-fields would be expected to subside considerably.

[16] κ_{const} was set to 200 as a rough estimate. In respect to correlation coefficients, this number is irrelevant.

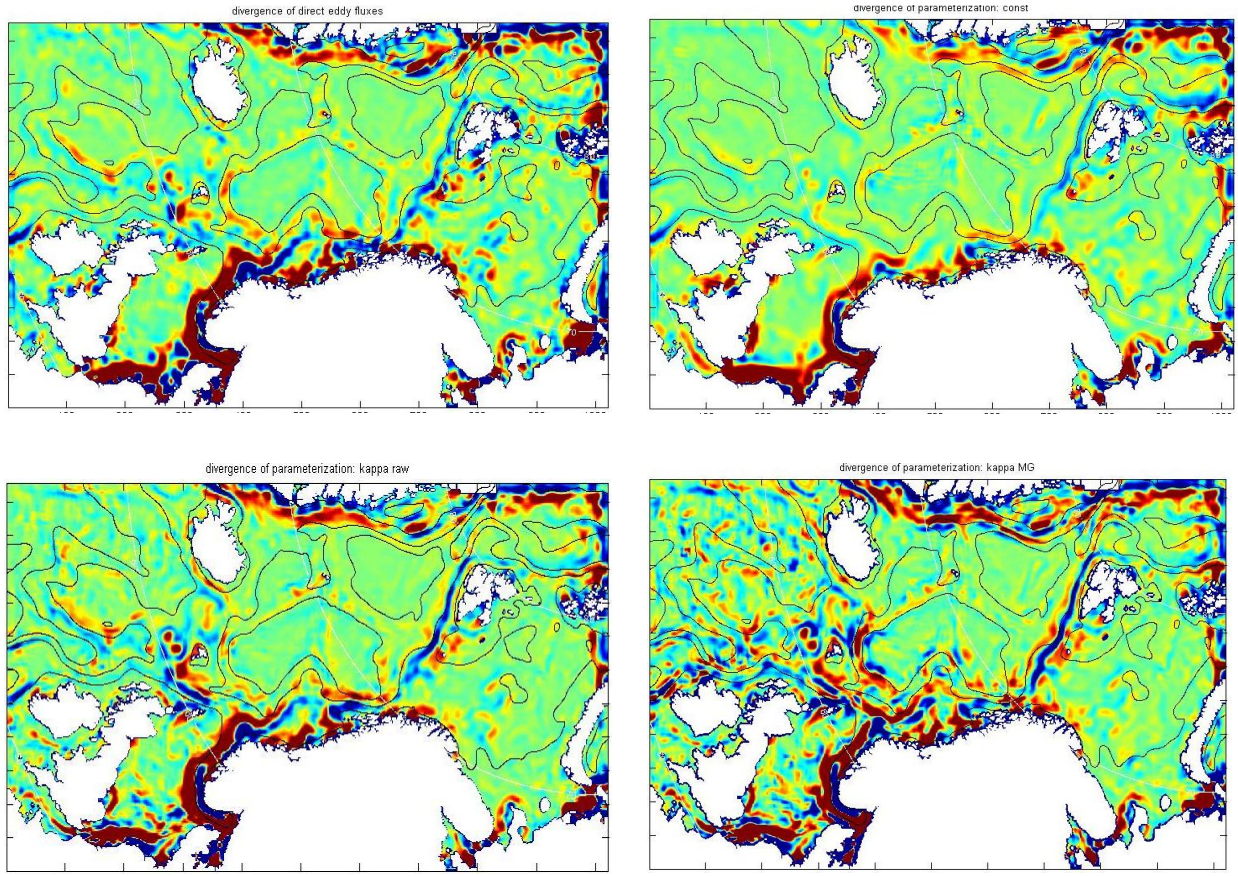

Figure 4.12a; Shown are the surface values of divergences of eddy density fluxes $\nabla \cdot \overline{\mathbf{u}'\rho'}$ *(upper left), and divergences of the downgradient parameterization* $\nabla \cdot (-\kappa \nabla_H \bar{\rho})$ *for* κ *as constant values (upper right), direct raw diagnostic (bottom left) and direct MG diagnostic (bottom right). Divergences are calculated (from the time averaged fields) at the end of the integration period.*

A surprisingly decent correlation obtained by the use of constant diffusivities (Figure 4.12b) indicates that the horizontal potential density gradient is the dominating factor in the left hand side of (47). It is obvious that, if diffusivities are generally positive, a choice of positive constant κ will generally produce divergence/convergence at the right places, but will most likely over- or underestimate the amount.

Hence, as expected, the closures (Figure 4.12b) also produced divergence fields resembling that of the eddy fluxes. To a varying degree they all describe the convergences along the WSC and the NAC belt south of the Faroe Islands, bordering to regions of large values of opposite sign. The strong coastal divergences are also prominent in the result. One of the pronounced features common for all cases is the trail of negative divergences (convergences) that appear in the NAC and WSC regions. This can be, ignoring salinity, attributed to the eddies' function of

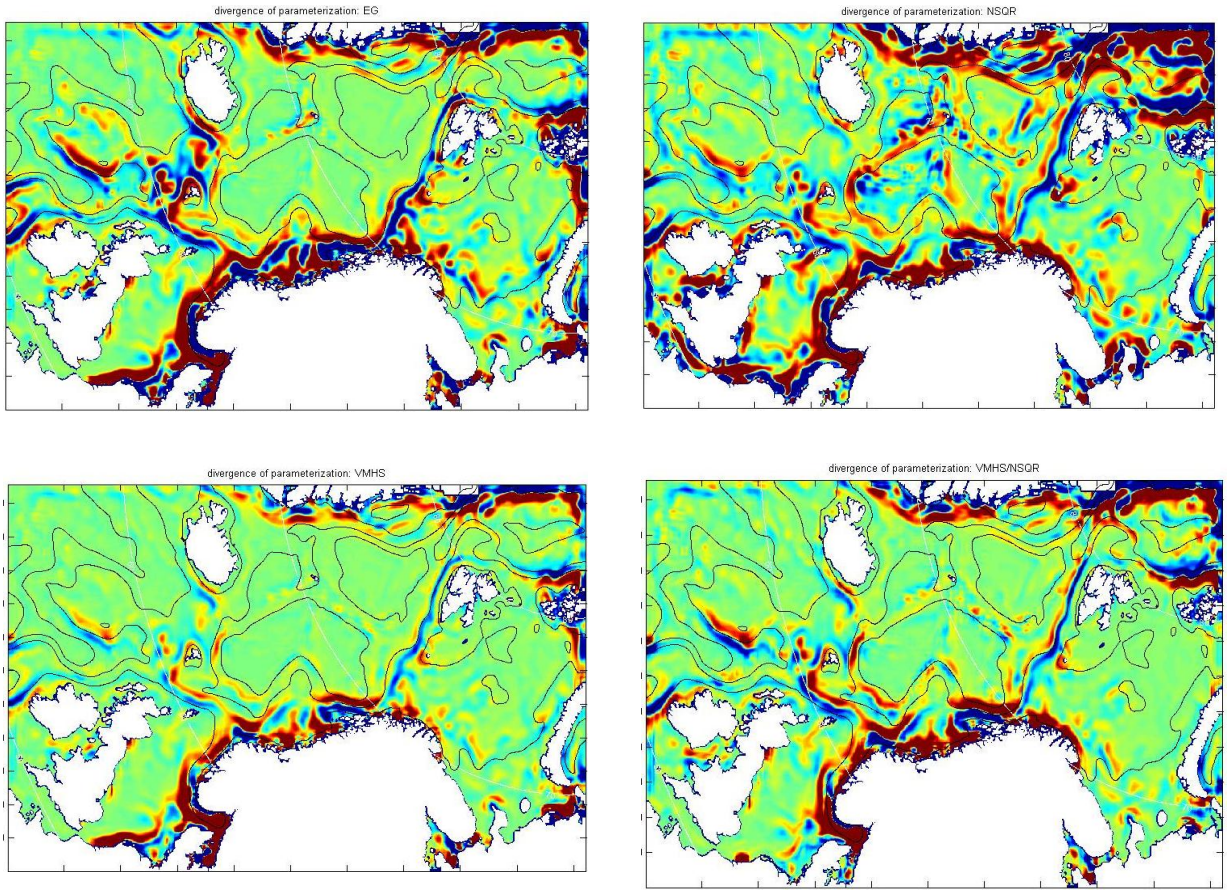

Figure 4.12b; Shown are the surface values of the downgradient parameterization $\nabla \cdot (-\kappa \nabla_H \bar{\rho})$ *for* κ *as EG (upper left), NSQR (upper right), VMHS (bottom left) and VMHS/NSQR (bottom right). Divergences are calculated monthly and averaged.*

distributing heat to surroundings[17], effectively cooling the warm currents and ultimately acts to increase local density. This process appears as a convergence of eddy fluxes in the warm current regions. Oppositely, strong divergence of eddy fluxes appear along parts of the costs of Greenland, Norway and Netherlands, suggesting that eddies contribute to warm up cold coastal waters.

The divergences as seen in Figure 4.12 are surface values computed at the very end of the integration period based on the obtained (monthly averaged) fields of κ and eddy-fluxes.

[17] In the cold Nordic Seas, salt is a significant contributor to the non-linear equation of state. But density fluxes is still dominated by temperature changes.

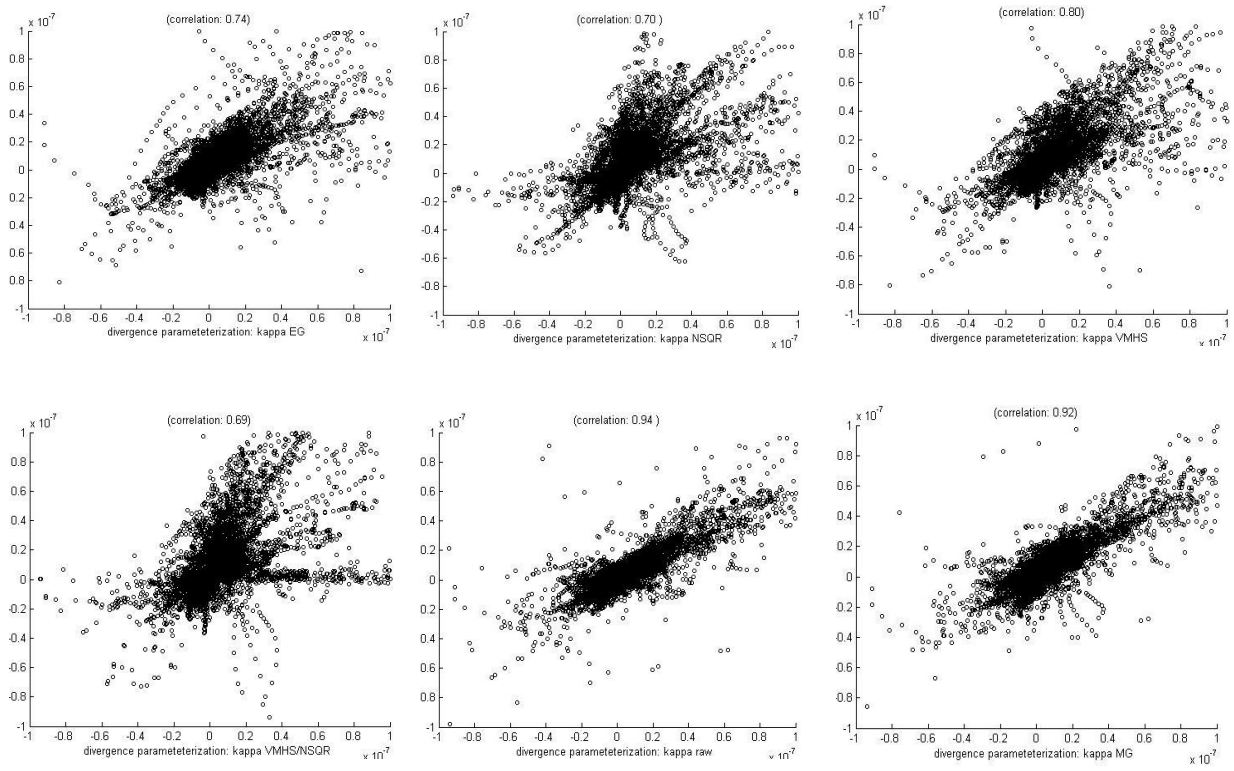

Figure 4.13; Correlations between the divergence of the eddy fluxes, $\nabla \cdot \overline{\mathbf{u}'\rho'}$, and the downgradient parameterization using various inputs of the mixing parameter κ. From top left, EG, NSQR, VMHS, VMHS/NSQR, raw, MG. The data are smoothed over 20 grid-points (associated with the rightmost column of Table 4.1.

Figure 4.13 illustrates the correlations obtained from this approach. To test closures and diagnoses under different circumstances, also divergences for both surface and depth averaged κ- and eddy fields are computed monthly and averaged over. The results of these different procedures for obtaining the divergences are summarized in Table 4.2 as correlation coefficients between the eddy flux and the downgradient parameterization with different input of κ. Once again, two different levels of spatial smoothing are applied, 3×3 (Lo) and 20×20 (Hi) grid points, for each case. The latter eliminates all signs of mesoscale physics, but as appropriate for coarse resolution models, only the large scale characteristics of the field is retained. The presented correlation coefficients demonstrate that the raw diagnostic of κ gives the best, and surprisingly strong, correlations based on divergences. Indeed, they are not perfect, and it may still exist another distribution of κ that would produce even higher correlations. But the fact that κ_{raw}, with rotational fluxes irrelevant due to the divergence, still grants better correlations than κ_{MG}, indicates that the MG method did

	Divergences calculated each month				Divergences at end of integration period			
	a) depth-avg		**b)** surface		**c)** depth-avg		**d)** surface	
Smoothing	Lo	Hi	Lo	Hi	Lo	Hi	Lo	Hi
EG	0.41	0.54	0.58	0.77	0.30	0.40	0.54	0.76
NSQR	0.39	**0.55**	0.57	0.83	0.39	0.58	0.51	0.70
VMHS	0.36	0.49	0.62	0.81	0.36	0.49	0.63	0.80
VMHS (FS)	0.36	0.49	0.62	0.80	0.37	0.51	0.64	0.81
VMHS/NSQR	0.37	0.49	0.52	0.79	0.34	0.52	0.52	0.69
κ raw	**0.46**	**0.55**	**0.71**	**0.90**	**0.52**	**0.76**	**0.75**	**0.94**
κ MG	0.46	0.52	0.68	0.88	0.33	0.46	0.69	0.92
Const.	0.34	0.49	0.64	0.81	0.32	0.43	0.64	0.74

Table 4.2; Correlation coefficients between the divergence of direct eddy fluxes and the divergence of the parameterization using different input values for the diffusion coefficient. Case a) shows the mean of all divergences calculated monthly (based on depth averages) for surface variables Case b) is the same, but instead of depth averages, surface values are used. In case c), the divergences are calculated at the end of the integration period (the eddy fluxes and direct diffusivities are still estimated each month). The Lo and Hi case refers to the amount of spatial smoothing done before estimating the coefficients, where Lo is 3 grid points and Hi is 20 grid points.

not work properly in this particular case (at least in terms of arranging for a better diagnosis by removing rotational components). EG and VMHS/NSQR, the two closures being both horizontally and vertically dependent, seem to perform equally well in general, with EG doing better on surface estimates VMHS/NSQR better in other depth-averaged cases.

One should be cautious when interpreting correlation coefficients in plain numbers. Since they are computed using a covariance (product of deviations from the respectable means), a set of evenly distributed numbers will generally score better than numbers varying with correct magnitudes (of varying sign) but also slightly displaced or "out of phase". This may have granted case Const., and to a certain degree NSQR, better ratings than deserved, and adversely with the somewhat noisy κ_{MG}, also suffering from some extreme peak values. Hence one should always use

correlation coefficients complimentary to more direct representations of data, e.g., Figure 4.12.

Section 5: Summary and discussion

5.1 General eddy distribution in comparison with the closure schemes.

The diffusivity parameter κ, appropriate for GM stirring (skew flux) and isopycnal diffusion, were diagnosed directly from the output of an eddy resolving model in order to learn more about the effect of mesoscale eddies associated parameterizations. Climate models are highly sensitive to their SGS operators, so the distribution of diffusivities is consequently pivotal to the integrity of predictions. With this in mind, a selection of closures designed to provide a large scale, flow-dependent approximation of the distributions were examined and tested in comparison with diagnoses taken in a high resolution domain.

Diagnoses affirmed that diffusivities have a vertical decay and strong topographic dependencies. More energetic eddies (and thus higher diffusivity) forms along boundary currents where gradients and horizontal velocity shears are large (here depth averaged diffusivities have magnitudes of κ~800 m^2/s, intensifying to well over κ~2000 m^2/s at the surface). Under such conditions barotropic instability may supply energy for eddies. Strong currents tend to 'shed' eddies, meaning, vortices may be formed and advected into regions with little instability (Vallis, 2005), which may be a contributory reason for the sturdy presence of diffusivities in the Barents Sea. Weak diffusivities, κ~50 m^2/s, are observed in deep water basins where EKE is low and stratification dominates shear forces. Surface values in such regions takes on a typical magnitude of 300 m^2/s, and could be anticipated to be heavily influenced by wind-forcing.

The various closure schemes were evaluated by their performance by comparing them to a), the direct diagnostic, and b), the divergences of eddy fluxes and the downgradient parameterization. Some adjustments were made to adapt them to the conditions of our model, discussed in Section 2.3.

The well-used VMHS (featuring depth-constant diffusivities) closure proved its advantage in the depth-averaged case. But obviously enough, vertical distribution and surface magnitudes were lacking. Diagnoses suggest that diffusivity should be high in upper layers and decaying with depth, consistent with observational data[18]. The utility of VMHS thus directly depend on how sensitive solutions are to horizontal contra vertical distribution of diffusivities. The answer to this may depend on the particular model and its domain, opting for choosing the most fitting closure, but in general we should expect that the vertical distribution plays a crucial role for evolution of the water masses. In respect of both observational physics and our result, we can at best only recommend this closure under special circumstances where depth varying mixing is considered to be of secondary importance. The closure EG seems to be the next best choice in light of the depth-averaged case, with a balanced bias and fewer extreme misses than the two remaining closures (Figure 4.10). Compared to our calculations, the tuning parameter c could be reduced from 2 to 1.5. A strange artifact with increasing near-bottom diffusivities appeared (Figure 4.8), likely formed because to the vertical velocity shear. As there is no outstanding argument for eddy diffusivities to increase near topography, and it did not show up in the direct diagnostic, we conclude with this being unphysical. This should however be a trivial problem to overcome during implementation.

Eden et al. 2007 finds NSQR to be less accurate in horizontal distribution than VMHS and EG, consistent with results in Section 4. At the same time, we found that the constant κ_0=4000$^{m^2}/_{s}$ vastly overestimated diffusivities on general basis (high values to appear in every column of water are not expected). We suggest reducing this to under 2000$^{m^2}/_{s}$. The overestimation was despite the fact that we used a denominator (N_{REF}) that was slightly higher than intended (the buoyancy inside the pycnocline). NSQR is nevertheless a simple closure that acutely reconstructs the amount of vertical decay observed in the diagnosis, better than the EG closure, which reduces κ too quickly beneath the surface layer. Again, depending on how sensitive climate models are on horizontal contra vertical spread of κ, our suggested closure VMHS/NSQR,

[18] Treguier et al (1997) also presents a theory based on linear baroclinic instabilities in which the diffusivity obtains both a horizontal and vertical dependence.

i.e., instead of assigning the constant value κ_0 in NSQR, using the horizontal spread given by VMHS with a doubled tuning parameter, appears as a solid choice.

In verdict of the direct diagnosis comparison, it turns out that no closure is outstandingly and generally better than the other in all traits, so precaution must be practiced when choosing a closure based on the dynamical domain of the model. Based on the direct comparison, we concur with Eden et al. 2008 that the EG closure may seem to be a better solution than both VMHS and NSQR. We point out however, that both of these two closures have advantages over EG in the horizontal and vertical (respectively). We encourage therefore further consideration of the combination closure VMHS/NSQR and advice for a future closure performance tests on general circulation models to include this kind of closure. At the same time we point out that all closures have weaknesses and biases compared to the direct diagnostic. One of these defects were addressed by a variant of the *Ferrari-Nikarushin suppression* in which we assert to in this study. It did not eliminate, but reduced, the problem with overestimation along topographic ledges and in core currents, and visibly (but subtly) improved correlation coefficients (it had seemingly most effect on VMHS/NSQR), both in the direct comparison and in the divergence case.

NSQR, despite being the most inaccurate closure concerning distribution of κ, produced *divergences* surprisingly close to the divergences of the eddy-fluxes (Figure 4.11-4.13, Table 4.2). It was debated whether smoother values could have been advantageous concerning the correlation coefficient, and this being the reason why Const. (and to a certain extent NSQR) attain relatively high correlation coefficients despite the distinct deviation from diagnosed distributions. From the correlation coefficient alone, Const. actually seems a respectable choice, considering its simplicity. Even so, Wright (1997) showed that results in a global model were improved by the advancement to non-constant diffusivities, in that case VMHS[19]. The divergence experiment also seems to support this closure.

[19] Prompting the Hadley Centre to employ this scheme in climate simulations (Gordon et al., 2000).

5.2 On diagnostics and theoretics.

We emphasize again that these conclusions are based on the assumption that the obtained diagnostics are amply correct, meaning, that they reflect the essential physical properties we study.

First one may ask how much of the clutters and blotches of diagnosed diffusivities in (Figure 4.4) is numerical noise and how much is actual physics. In other words, would the noisy field compromise the credibility of the diagnosis? There is no preceding argument that the diffusivity present in the real ocean should take on a more constant value with smoother gradients (as turbulence behaves erratically, so can eddies on various scales). An inspired guess could be that the noise springs from bit of both; erratic eddy mixing as well as spurious noise that partly masks the signal. Regardless, if one were to use this kind of diffusivity diagnostic (as shown in Figure 4.4) a *priori* parameter choice for SGS parameterizations in coarse resolution models, the fields will have to be thoroughly smoothed. That is, local spatial averages converted into point values on the coarser grid. Averaging the solutions over reasonable scales should hopefully pick up the essential physics, eliminating the noise and consequently the need to explicitly address this question.

More importantly, one must be vary of the challenges arriving with interpreting direct diagnostics of diffusivities of the assumptions and complications it involves. We have assumed and addressed perturbations from a defined temporal mean flow as an effect of mesoscale eddies, and expect the horizontal downgradient parameterization to hold. In addition there are non-divergent rotational fluxes that may warp the integrity of estimates. In earlier studies diagnoses showing large and dominating negative diffusivities and poor flux-gradient correlations have been attributed to the presence of rotational fluxes (Bryan et al., 1999).
In our diagnostic using the raw eddy fluxes, we observed only occasional negative fluxes and otherwise physically plausible amounts of κ (despite the influence of rotational fluxes expected to thwart estimations). The dominating positive diagnosis is a consequence of the prevailing trend of eddy fluxes being directed down the mean gradient, ensuing after physically moderate spatial smoothing of the vector fields.

Utilizing the MG-method (Medvedev & Greatbatch 2004, Eden et al., 2006) in order to remove rotational components and retain residual divergent fluxes only, we found a general increase of magnitudes but also a rise of intense negative diffusivities in confined regions. This result was unexpected, seeing that getting rid of negative diagnoses of diffusivities has been a key motivation for attempts to separate divergent and rotational fluxes. There is not a straightforward reason for this inconsistency with e.g., Eden et al (2006). It is worth noting that in our case, estimations of κ_{raw} appeared as less noisy and more physically plausible when running the diagnosis after each temporal 'averaging window', i.e., the temporal mean to which we assumed perturbations to be eddy activity, and thereafter taking a final average of all κ_{raw} assimilated at the end of the five year run. There might have been a difference in our procedures and those of Eden et al. concerning this, but large regions of intense negative regions were not registered by our diagnostics after any attempted averaging routine.

Another source of aberration could be the different model and model type used in our study. Where geopotential models are extensively used in similar studies, an advanced terrain-follow coordinate model (ROMS) produced our data. Even models of the same coordinate system have distinctive dynamical properties, and differences in the source data could be a contributory reason for the deviating results. General non-existant negative diffusivities could also be a consequence the high resolution domain itself. More detailed topography (and starker gradients) may prompt eddy fluxes to become more downgradient, compelling (44) to produce positive κ.

A question that presents itself is how we interpret the negative diffusivities that persevere in all experiments. Certainly a large expanse of negative diffusivities would necessarily be unphysical. But in terms of stirring, it is not unthinkable that, in certain regions and topographic conditions, that mesoscale eddies could work towards increasing APE by consuming MKE, maintaining tilting isopycnals. In this case, a horizontal up-gradient eddy-flux could reside and generate negative diffusivities. A negative (positive) vertical eddy density flux $\overline{w'\rho'}$ is associated with eddies releasing (piling up) available potential energy (Eden et al., 2006). Figure 4.13 reveals certain

areas of positive vertical eddy flux. In a few places these seem to loosely cohere with regions of negative κ (Figure 4.5). The prospect of physical negative stirring beseeches attention in future studies, but is beyond the scope of this paper.

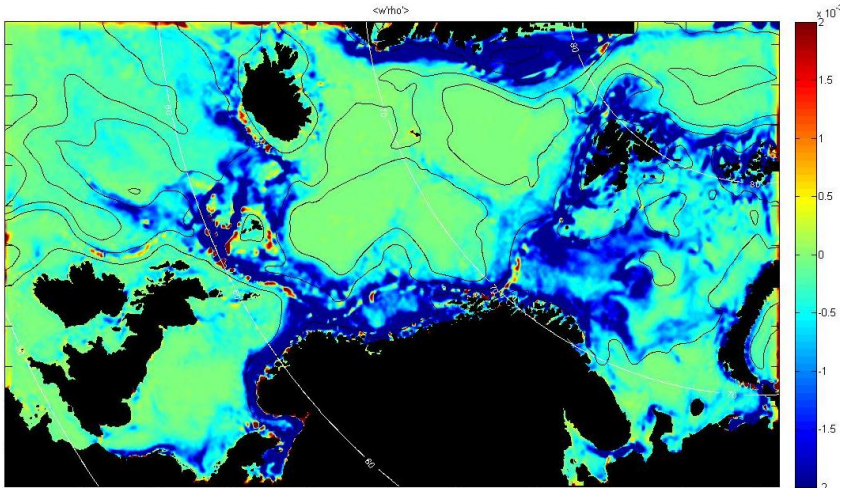

Figure 4.13; Vertical eddy density flux $\overline{w'\rho'}$.[20] *Negative values are associated with the release of APE due to eddy activity.*

To avoid the complicity and question of the rotational fluxes, we employed the divergences of the eddy fluxes and the parameterization. The flux-gradient correlation of the raw diagnosis appeared even more evident after employing the divergences of the eddy fluxes and the divergences of their downgradient parameterization. This is in contrast to several previous studies (e.g., Nakamura and Chao, 2000). Griesel et al., (2009) report of no evidence of correlation, even after various spatial averages, and question the validity of associating mesoscale eddies with a downgradient assumption. We emphasize based on observations in this study that the (isotropic) horizontal downgradient parameterization indeed seem to capture the general effect of the eddy fluxes. We note again however, that averaging over a range of eddy scales through spatial smoothing, improved the correlation. Hence, flux fields is seemingly another important factor, in addition to rotational fluxes, that may unsettle a clear manifestation of downgradient relationship.

The high correlation of the divergences of fluxes and parameterization obtained by using the κ_{raw} diagnosis, strongly supports the assumption that κ_{raw} is fair estimate

[20] *The vertical eddy flux is estimated as* $\overline{w'\rho'} = \overline{w}\,\overline{\rho} - \overline{w\rho}$.

of the actual distribution of the diffusivity coefficient, and an appropriate reference point for comparing the closures. In consequence, this suggests that rotational fluxes had less influence than expected on the direct diagnosis in this particular experiment. Actually, κ_{MG} that theoretically contains less rotational components, performed worse in premise of divergences (but still better than any of the closures), is a strong indicator that the MG-method did not work as intended in our experiment, despite several approaches and efforts to produce a "good" result.

Its noisiness may be a contributory reason for lower correlation scores, but it is also visible in Figure 4.12 that the raw field indeed correlates more. In addition to the implementation differences discussed above, one may speculate that be that the MG-method principally work over larger regions of negative diffusivities (depending on the size or scale of the variance fields), with the defect of inducing local amounts of negative diffusivities. In such a case, our limited region model, with few negative regions to begin with, could be a contributory cause of this unexpected development.

Griesel et al. raises the concern that if the rotational component is vastly dominating the divergent component (Bryan et al., 1999), extracting the small residual difference will be highly sensitive to small errors and require very precise methods. So even if perfectly implemented, the MG method is an approximation that does not necessarily remove all rotational components, attesting to that the task of describing the residual fluxes and their relative magnitudes correctly may in general be difficult. Alas, Eden et al., (2006, 2007) bring little specifics on the implementation and no other independent studies utilizing the MG method directly were found. It is however clear that extracting the divergent component requires high quality data, precise implementation methods and a solid physical theory.

On a different note, it has earlier been argued (Rix & Willebrand, 1996) that the timeframe of five years may be too short to get a good estimate of the eddy fluxes. This study indicates otherwise, and we emphasize that even shorter time series gave a decent representation of the results (granted the needed spatial smoothing). This assumed temporal sufficiency is consistent with Roberts and Marshall (2000), who

noted that the five-year mean indeed resembled and were representative for a twenty-year mean. This seems only natural, as the relevant time-scales of mesoscale eddies we investigate range from three weeks down to under a week (ref []). An adequate set of such processes should be captured in a five year mean. An extended period of time may however slightly reduce the need for spatial averaging or smoothing of data, but we see no practical (or even theoretical) incentive for this; the downgradient nature of eddy induced fluxes appeared clearly though physically reasonable use of smoothing windows.

5.3 Summary and final remarks.

In summary, this study shows a reasonable diagnostic of eddy diffusivities found using raw eddy fluxes (as confirmed by the divergence test), hence assumed to be adequate as a reference for comparison of the four tested closures. VMHS produces the best horizontal distributions but do not respect the vertical profile of eddy kinetic energies (and may be useful in for instance shallow simulation domains). EG and VMHS/NSQR have a horizontally and vertical advantage compared to each other, respectively, and score about equally well on the correlations of divergences. We encourage the suggested combination-closure as a possible candidate to be tested in coarse resolution experiments. NSQR, albeit its poor horizontal distribution of diffusivities, did produce commendable divergence fields. We cannot from these results dismiss any of the four as, in general, inferior to another. The utility of each closure seem to be situational and should be chosen for the specific application. On a different note, we recommend the use of a Ferrari-Nikarushin suppression when employing flow dependent closures as VMHS or EG, that slightly reduced the problem with overrepresented diffusivities along main currents and topographic slopes and increased correlations.

It was however found that the suggested tuning parameters for the closures were overestimated, especially for the NSQR case. Based on the result of diagnoses herein, a constant value of $\kappa \sim 400\, m^2/s$ seems more plausible than the commonly seen

κ~800 m^2/s. If our more moderate diagnoses of diffusivity magnitudes are domain-specific or reflect a general trend in the World Ocean, cannot be told from these our calculations. Nonetheless, it prompts for the use of high resolution analogues of models employing these closures to estimate the optimal value of tuning parameters prior to the coarse resolution run. Alternatively, as an approximation, it could prove useful to exert the high resolution diagnostic directly as a time independent distribution, if the general flow characteristics of the system is assumed to undergo little change during the integration time. For climate models of prolonged integration time where this is not the case, a periodically high resolution estimation could be considered.

Other implications of this study include affirmation of the validity of the horizontal downgradient assumption of eddy density fluxes, shown for both the fluxes themselves and the divergence.

Furthermore, it was discussed practical and theoretical difficulties of determining rotational and divergent parts using the MG method, or any method per se. If the rotational component proves to vastly dominate the divergent (at least in cases it does), approximations like the MS or MG theories may be inadequate to determine point values of residual fluxes. This study indicated however, that producing physically reasonable diagnoses of diffusivities using raw fluxes is possible if the eddy-fluxes are spatially smoothed over appropriate scales. A hypothesis of Griesel et al. (2009) speculates if averaging over certain spatial scales may cause some rotational components to cancel out. If possible, this may have been a contributory reason for the seemingly mild influence of rotational fluxes on our diagnosis of the eddy mixing parameter κ.

It has been a strong focus on the topic of diffusivity diagnostics from high resolution ocean models. We encourage future assessment as to why the eddy fluxes seemingly behaved so differently in this study, with strong flux-gradient correlations despite the presumed presence of rotational fluxes. More specifically, this type of model and configuration could be applied to other regions and diffusivities assessed in similar studies to compare physical diagnostics from different approaches and shed more light on the subject. Is the appropriate spatial smoothing of eddy fields defined as

deviations from monthly temporal means always able to produce plausible diagnostics of κ (using these model configurations) regardless of rotational fluxes, or is it characteristic for the Nordic Seas? The same question applies to the seemingly non-functional MG-theory in our experiment. Would it work on larger domains as exercised in Eden et al., (2006) and Eden, (2007), or would a different model and configuration produce any different diagnoses in the Nordic Seas? Would we find the same magnitude of diffusivities as diagnosed by Eden et al (2006) in the North Atlantic if we applied the procedures practiced here?

A wide spectrum of models and observations is needed to solve the mesoscale problem, and studies should aim to work synergistically. As mentioned in the introduction, the current study is more theoretical than the experiments of Eden et al., (2008), in the sense that we do not know which diffusivity diagnose that actually works the best before having tested it in a climate model, which of course is the final goal with these estimates; better model input. Comparing the results of the climate model with climatology, however, may pose too many arbitrary factors to give sufficient information specifically about the tested closure. One of the factors overshadowing this is, of course, is the dynamics of the climate model in itself. To rule such factors out one could study satellite data or actual drifters in the ocean, something that brings with it its own difficulties and caveats.

Each approach of research contributes with its own advantages and uncertainties, and we should aim to use several approaches toward each goal. The result of this study will hopefully be of some use as a reference for future research of mesoscale dynamics in the Nordic Seas.

References

Arakawa, A & Lamb, (1977) Computational design of the basic dynamical process of the UCLA general circulation model.

Bryan, K., J.K. Dukowicz, and R.D.Smith, 1999; On the mixing coefficient in the parameterization of bolus velocity. *J. Phys. Oceanogr.*,, 29, 2442-2456.

Chelton, D. B., R. A. Deszoeke, M. G. Xchlaz, K. E. Naggar, and N. Siwertz, 1998: Geographical Variability of the first baroclinic Rossby Radius of deformation. *J. Phys. Oceanogr, 28, 433-460.*

Chelton et al.,, R. M. Samelson, and R. A. de Szoeke, 2007: Global observations of large oceanic eddies. Geophys. Res. Lett., 34,L15606

Danabasogu, G., and Marshall J., (2007) Effects of vertical variations of thickness diffusivity in an ocean general circulation model.

Eden, C., Jochum, M., Danabasoglu, G., 2008: Effects of different closures for thickness diffusivity.. *Elsevier, Ocean Modelling.*, 26, 47-59.

Eden, C., 2006: Thickness diffusivity in the Southern Ocean, *Geophys. Res. Lett.*, 33, L11606, doi:10.1029/2006GL026157.

Eden, C., R.J. Greatbatch and J. Willebrand, 2007b: A diagnosis of thickness fluxes in an eddy-resolving model. *J. Phys. Oceanogr, 37, 1282-1296.*

Eden , C., and Greatbatch R. J., (2008) Towards a mesoscale eddy closure. Ocean modelling, 20, 233-239.

Ferrari, R., Nikarushin, M., 2010: Suppression of Eddy Diffusivity across Jets in the southern ocean *J. Phys. Oceanogr, 40, 1501-1519*

Fox-Kemper, B., R. Ferrari and J.Pedlosky, 2003. A note on the indeterminacy of rotational and divergent fluxes. *J. Phys. Oceanogr.*,, 33, 478-483.

Gent, P.R., and McWilliams J.C., (1990). Isopycnal mixing in ocean circulation models. *J. Phys. Oceanogr.*,, 20, 150-155.

Gent et al., (1995) Parameterizing eddy induced transports in ocean circulation models. *J. Phys. Oceanogr.*, 26, 463-474.

Gerdes, R., 1993: A primitive equation ocean circulation model using a general vertical coordinate transformation. 1. Description and testing of the model. *Journal of Geophysical Research, 98, 14683-14701.*

Gordon, C., C. Cooper, C. A. Senior, H. Banks, T. C. Gregory, J.F.B Mitchell and R.A. Wood, 2000: The simulation of SST, sea ice extents and ocean heat transports in a version of the Hadley Centre coupled model without flux adjustments. *Climate Dynamics , 16,* 147-168.

Green, J. A., 1970: Transfer properties of the large scale eddies and the general circulation of the atmosphere. Quarterly journal of Royal Meteorological Society

Griesel., A., Gille, T., Sprintall, J., McClean, J., and Maltrud, E. M. 2009: Assessing eddy heat flux and its parameterization: a wavenumber perspective from a 1/10° ocean simulation. *Elsevier, Ocean Modelling.*, 29, 248-260.

Griffies, Stephen M (2004) Fundamentals of Ocean Climate Models (Princeton University Press)

Griffies, Stephen M. (1998) The Gent McWilliams Skew Flux. *J. Phys. Oceanogr.*, 20, 1634-1637.

Haidvogel, D.; Arango, H.; Budgell, W.P; Cornuelle, B.D, Churchitser, E.; Lorenzo, E. Di; Fennel, K.; Geyer, W.R.; Hermann, A.J.; Lanerolle, L.; Levin, J.; McWilliams, J.C.; Miller, A.J.; Moore, A.M.; Powell, T.M.; Shchepetkin, A.F.; Sherwood, C.R.; Signell, R.P.; Warner, J.C and Wilkin, J. (2008). Ocean forecasting in terrain-following coordinates: Formulation and Skill-assessment of the Regional Ocean Modeling System. Journal of Computational Physics, Vol. 227: p. 3595-3624.

Iselin, C.O., (1939). The influence of vertical and lateral turbulence on the characteristics of the waters at mid-depths. Eos. Trans. AGU, 20, 414-417.

IMCS (2008) Regional Ocean Modelling System (ROMS). Web; www.myroms.org Institute of Marine and Coastal Sciences, Rutgers University.

McDougall, T. J., (1987) Neutral Surfaces. *Journal of Physical Oceanography*, 17, 1950-1964.

Jackett, D. R. and T. J. McDougall, 1995: Minimal Adjustment of Hydrostatic Profiles to Achieve Static Stability, *J. Atmos. Oceanic Techn.*, **12**, 381-389.

Jayne, S. R., and J. Marotzke, 2002: The Oceanic Eddy Heat Transport. *Journal of Physical Oceanography*, Vol. **32**, pp. 3328-3345.

Marshall, J., and G. Shutts, 1981: A note on divergent and rotational eddy fluxes. *Journal of Physical Oceanography, 11, 1677-1680.*

Medvedev, A.S., Greatbatch, R.J, 2004: On advection and diffusion of the mesosphere and lower thermosphere: The role of rotational fluxes. *J. Geophys. Res., 109.*

Mellor, G. L. and T. Yamada, 1982: Developement of a turbulence closure model for geophysical fluid problems, *Rev. Geophys. Space Phys.*, **20**, 851-875.

Nakamura, M., and Y. Chao, 2000: On the eddy isopycnal thickness diffusivity of the Gent-McWilliams subgrid mixing parameterization. *J. Climate*, **13**, 502–510.

Papanicolaou, G., and O. Pironneau, 1981: On the asymptotic behaviorof motion in random flows. Stochastic Nonlinear Systems,L. Arnold and R. Lefever, Eds., Springer, 36–41.Pedlosky, J., 1987: Geophysical Fluid Dynamics. 2nd ed. Springer

Pedlosky, J., 1987: Geophysical Fluid Dynamics. 2nd ed. Springer

Reif, F., 1965: Fundamentals of Statistical and Thermal Physics. McGraw-Hill.

Redi, M. H., (1982) Oceanic isopycnal mixing by coordinate rotation. J. Phys. Oceanogr, 12, 1154-1158

Rix, N.H., Willebrand, J., 1996. Parameterization of mesoscale eddies as inferred from a high-resolution circulation model. *J. Phys. Oceanogr., 26, 2281-2285.*

Røed, Lars Petter, (2009 revision) Fundamentals of Atmospheres and Oceans on computers. Syllabus compendium at University of Oslo.

Roberts, M., and Marshall D., (1998) Do we require adiabatic dissipation schemes in eddy-resolving ocean models? Journal of Physical Oceanography, 28, 2050-2063.

Roberts, M., and Marshall D., (2000) On the validity of downgradient eddy closure in ocean models. *J.*

Phys. Oceanogr., 105, 28613-28628.

Shchepetkin, A. F., and J. C. McWilliams, 2005: The Regional Ocean Modeling System: A split-explicit, free-surface, topography following coordinates ocean model, *Ocean Modelling*, **9**, 347-404.

Solovev, M., Stone, P.H., Malanotte-Rizoli., 2002. Assessment of the mesoscale eddy parameterizations for a single basin coarse-resolution model. *J. Phys. Oceanogr., Res. 107, 3126.*

Treguier,A.M., 1999: Evaluating eddy mixing coefficients from eddyresolvingocean models: A case study. J. Mar. Res., 57, 89–108.

Tanaka, Y., Hasumi, H., Endoh, M., 2007. The distribution of the thickness diffusivity inferred from a high-resolution ocean model

Veronis, G., (1975) The role of ocean models in tracer studies. Numerical models of Ocean Circulation, Natl. Acad. Sci., 133-146.

Visbeck, M., J. C. Marshall, T. Haine, and M.Spall, 1997: Specification of eddy transfer coefficients in coarse resolution ocean circulation models. *J. Phys. Oceanogr, 27, 381-402.*

Wunch, Carl & Rafaele, Ferrari (2004) Vertical Mixing, Energy, and the General Circulation of the Oceans. Annu. Rev. Fluid Mech., Vol 36: p. 281-314.